NOVEL CHARACTERISTICS OF SMALL NONCODING RNAS IN RAT EPIDIDYMAL EXTRACELLULAR PARTICLES

Running Head: Small noncoding RNAs in rat epididymal particles

Keywords: sncRNA, extracellular vesicles, epididymis, epididymosomes, miRNA, tRNA fragments, CpG island, rat

Ross Gillette[1], Dana L. Sheinhaus[1], Shyamal Waghwala[1], Andrea C. Gore[1†]

[1] The Center for Molecular Carcinogenesis and Toxicology, Division of Pharmacology and Toxicology, College of Pharmacy, The University of Texas at Austin, Austin, TX, 78712, USA

Ross Gillette: https://orcid.org/0000-0002-1296-8428
Andrea C. Gore: https://orcid.org/0000-0001-5549-6793

AUTHOR CONTRIBUTIONS

Conceptualization: R.G.; Methodology: R.G., D.L.S.; Investigation: R.G., D.L.S.; Formal Analysis: R.G., S.W.; Writing – Original Draft: R.G.; Writing – Review & Editing: R.G., D.L.S., A.C.G.; Funding Acquisition: R.G., A.C.G.

[†] Corresponding Author: andrea.gore@austin.utexas.edu

ABSTRACT

Extracellular vesicles (EVs) released from the epididymal epithelium, referred to as epididymosomes, impart functional competence on sperm as they transit the epididymis by merging with sperm and releasing a complex repertoire of molecules. The cargo of epididymal EVs includes small noncoding RNAs (sncRNAs) that are modified by external factors such as stress, nutrition, and drug use, which are delivered to sperm and affect offspring development and outcomes. The rat is an important translational model system for many fields including reproduction and transgenerational epigenetics, but there is little work on rat epididymosomes and their sncRNA cargo. To fill this gap in knowledge, in the current study we performed a comprehensive characterization of an epididymal EV preparation that we refer to as extracellular particles (EPs) because of the potential presence of other non-vesicular extracellular particles along with the EVs. EPs were collected from the caput epididymis, isolated, subjected to verification of the presence of EVs, and sncRNAs were sequenced. We considered nearly all known categories of small RNA and their fragment sub-types and in the process identified a subset that did not strictly fit the definition of any known category. These unique small RNAs are expressed strictly from within the boundaries of CpG islands and have a distinct 19-nt length. Their functional significance remains unknown, but they have characteristics of RNA fragments that can associate with the Argonaute/PIWI family of proteins and therefore could have regulatory function via RNA induced silencing or de novo DNA methylation.

21 **INTRODUCTION**

22 Spermatozoa are incapable of fertilization as they exit the testes [1] and only gain motility
23 and the capacity for fertilization as they transit the epididymis from the caput to the cauda [2]. This
24 process requires epididymosomes [3–6], a type of extracellular vesicle (EV) within the
25 microvesicle category [7–9]. Epididymosomes are released from the epididymal epithelium via
26 apocrine secretion [10], fuse to spermatozoa [11], aid in their maturation and functionalization
27 [4,12,13], and mark dead or dying spermatozoa for elimination [14,15]. Epididymosomes carry a
28 complex repertoire of ions, proteins [16], phospholipids [17], metabolites [18], and small non-
29 coding RNAs (sncRNA) [4,12,19,20] that are transferred to [21,22] and alter the function of the
30 spermatozoa or impart functional consequences on the fertilized embryo [23]. Importantly,
31 sncRNA molecules transferred to spermatozoa have the capacity to alter the epigenetic landscape
32 of either the spermatozoa or the fertilized embryo and thereby influence subsequent generations
33 [22,24]. Furthermore, the sncRNA contents of epididymosomes are subject to modification by the
34 hormonal milieu [25,26] and environmental challenges such as psychosocial or metabolic stress
35 [26–31], making them a potential vector for intergenerational effects in offspring. This key role
36 was illuminated by studies showing that early life stress caused behavioral and physiological
37 changes in the offspring, phenotypes that were recapitulated by microinjection of a small number
38 of microRNAs into a fertilized egg subsequently used for *in vitro* fertilization [24,32,33].

39 The sncRNA repertoire of epididymosomes is complex and diverse, with most information
40 in model systems from mice [34]. The most abundant sncRNA found in mouse epididymosomes
41 is microRNA (miRNA) followed by smaller proportions of transfer RNA (tRNA) and ribosomal
42 RNA (rRNA) [29,34,35]. The remainder consists of piwi-interacting RNA (piRNA), small nuclear
43 RNA (snRNA), and small nucleolar RNA (snoRNA) [29]. Other species of sncRNA, such as Y
44 RNA and Vault RNA, have not yet been reported in epididymosomes but should not be ruled out
45 for inclusion in these complex profiles. Furthermore, there are likely additional sncRNAs yet to
46 be identified [36].

47 Much of the knowledge we have on the sncRNA contents of caput epididymosomes, which
48 are crucial for the final steps of spermatozoa maturation, is from mouse models [29,34,35].
49 However, there is minimal conservation between the miRNA in caput EVs between mice and
50 humans [37] and to our knowledge, other classes of sncRNAs have not been directly compared
51 between species. Very little has been reported on the epididymosomes of rats, which are an
52 important model system for endocrinology, reproduction, and epigenetic transgenerational
53 inheritance, and in which behavioral work is considered to better translate to humans [38–40].
54 Here, we characterized the contents of EPs derived from the caput epididymis of the male rat,
55 during which we identified what we believe to be a previously undefined class of sncRNA.

56

57 **MATERIALS AND METHODS**

58 **Animals and treatment**

59 All animal experiments were conducted using humane procedures that were approved by
60 the Institutional Animal Care and Use Committee at The University of Texas at Austin and in
61 Accordance with National Institutes of Health (NIH) and Animal Research: Reporting of *In Vivo*
62 Experiments (ARRIVE) guidelines [41]. Three-month old male and female Sprague Dawley rats
63 were purchased (Envigo, Indianapolis, IN) and shipped to the Animal Resource Center at the
64 University of Texas at Austin and allowed two weeks to acclimate to the housing facility. All
65 animals in the colony were housed in a room with consistent temperature (~22° C) and light cycle
66 (14:10 light:dark), had *ad libitum* access to filtered tap water and a rat chow with minimal
67 phytoestrogens (Teklad 2019: Envigo, Indianapolis, IN), and housed in cages lined with wood-
68 chip bedding (Sani-Chips: P.J. Murphy, Montville, NJ). After acclimation, female rats were
69 observed for vaginal cytology as previously described [42,43] indicating proestrus, and therefore
70 receptivity. Receptive female rats were randomly paired with an experienced breeder male,
71 receptivity was confirmed via the observation of lordosis during a mount, and the pair was left
72 together overnight. The following morning, vaginal cytology was checked for the presence of

73 sperm and if present, the animal was marked as embryonic day (E1). The pregnant dams were
74 single-housed and provided nesting material on E18.

75 On E8, the dams (N = 6) were randomly split into two groups (each N = 3) and fed ¼ Nilla
76 Wafers™ daily with either 3% DMSO or 1 mg/kg Aroclor 1221 (A1221) (#C-221N,
77 Accustandard, Lot #072-202-01 - an estrogenic polychlorinated biphenol [44]) from E8 – E18 and
78 postnatal day (PND) 1 – 21. The original goal of work was to characterize sncRNAs in rat
79 epididymal EVs, as well as to generate pilot data on effects of the endocrine-disrupting chemical,
80 A1221. However, no differential expression of sncRNAs was caused by treatment after corrections
81 for multiple comparisons. Therefore, treatment was not considered or analyzed in any of the data
82 presented in this manuscript with current work focused solely on characterization of the
83 composition of EV sncRNAs. Litters were culled to 5 females and 3 males based on median
84 anogenital index at P1. At PND 21, all pups were weaned and housed in cages of two or three
85 same-sex animals. Only males were used in the present manuscript and were otherwise
86 unmanipulated until euthanasia besides weekly handling to acclimate each rat to the experimenters
87 in order to reduce stress. Females were allocated to other projects.

88

89 **Sample Collection**

90 At PND 105, one male rat was randomly selected from each of the 6 litters using a random
91 number generator (N = 1 per litter) and euthanized by rapid decapitation. The testis and epididymis
92 were removed via a small incision in the scrotum. The epididymis was separated from the testis
93 and segmented into three portions (caput, corpus, and cauda). The caput of the epididymis was
94 minced into small pieces with scissors and placed in warm (37° C) M2 culture media (M7167,
95 Millipore Sigma) with HEPES (5.43 g/L) and 2% exosome depleted fetal bovine serum
96 (A2720803, ThermoFisher). The slurry was placed on a rocker at room temperature for 30 minutes
97 to allow sperm and epididymal fluid to suspend in solution, the supernatant was removed and large
98 tissue chunks were excluded. The resulting supernatant was centrifuged at 500 X g for 5 minutes

99 to pellet and remove sperm. The supernatant was again removed, immediately frozen on dry ice,
100 and stored at -80° C until use (~ 3 mo) which is the preferred method of storage when necessary
101 [45] and within the timeframe before which substantial effects to EVs are observed [46].
102

103 **Extracellular Particle Purification and Nucleic Acid Extraction**

104 The buffer supernatant containing extracellular particles from the caput of the epididymis
105 was thawed on ice for 30 minutes prior to isolation. When fully thawed the buffer was mixed by
106 pipetting and then filtered with a 0.8 µm syringe filter (Millex-AA, SLAA033DD, Millipore
107 Sigma) to remove any cells or large cellular debris. Extracellular particles and RNA were
108 sequentially isolated from the media using the Qiagen exoRNeasy Midi kit [47] (#77144, Qiagen,
109 Germantown, MD) according to the manufacturer's protocol. Briefly, 200 µl of media from each
110 sample was passed through a spin column that selectively binds extracellular vesicles. The column
111 was washed to remove contaminants and debris, and then eluted in Qiazol lysis buffer (#79306,
112 Qiagen, Germantown, MD). Chloroform (AAJ67241AP, FischerScientific) was added, mixed by
113 shaking, and incubated at room temperature to allow phase separation. Phase separation was aided
114 by centrifugation at 12,000 X g for 15 minutes at 4° C and the aqueous phase was aspirated and
115 passed through a second membrane spin column that selectively binds RNA. The membrane was
116 washed to remove contaminants and the sample eluted in 13 ul RNase free water. M2 culture media
117 and 2% exosome depleted fetal bovine serum was used as a negative control to determine
118 exogenous contamination and subjected to the same extracellular vesicle and RNA isolation
119 procedures described above. These negative controls were analyzed via particle analysis and for
120 resulting nucleic acids to ensure there were no exogenous or contaminating exosomes or nucleic
121 acids. None were found (**Supplemental Figure S1A**).
122

123 **Extracellular Particle and RNA Quality Control**

124 An aliquot of the extracellular particles from the same samples described above were
125 isolated using the exoEasy Maxi Kit (76064, Qiagen) according to the manufacturer's protocols.
126 The resulting EPs from two samples were analyzed using a NanoSight 300 (Malvern Panalytical)
127 in 5 replicates to establish a size distribution of the resulting EPs and to ensure there were no
128 contaminating particles. RNA extracted from isolated EPs was first quantified (ND-1000,
129 ThermoScientific) and diluted for size distribution analysis and quality control using the small
130 RNA (5067-1548, Agilent) and pico RNA kits (5067-1514, Agilent) on a BioAnalyzer 2100
131 (Agilent). We found there was no cellular contamination indicated by a lack of 18s and 28s
132 ribosomal RNA [48,49] and that the majority (~80%) of extracted RNA was in the 20-40 bp range,
133 indicative of small RNA molecules (**Supplemental Figure S1B**).

134

135 **Characterization of Extracellular Particles by Electron Microscopy**

136 Transmission electron microscopy (TEM) and cryo-electron microscopy (cryo-EM) were
137 performed at the University of Texas's Center for Biomedical Research Support (CBRS). TEM
138 specimens were pre-fixed in microfuge tubes by adding 0.1 µl of electron microscopy grade 16%
139 paraformaldehyde (Electron Microscopy Sciences) to 5 µl purified specimen and incubating for
140 20 minutes at room temperature. Negative staining was performed by applying 5 µl of pre-fixed
141 sample to a glow discharged grid and allowing to adhere for 1-2 minutes, then washed on a drop
142 of molecular grade water, stained with 2% aqueous uranyl acetate, blotted, and allowed to dry prior
143 to imaging in an FEI BioTwin electron microscope fitted with an AMT 1kx x 1kx camera.

144 Cryo-EM specimens were applied to a glow-discharged lacey carbon grid. The grid was
145 incubated for 30 seconds at 4° C and blotted with filter paper to leave only a thin film spanning
146 the grid holes. The sample was kept at 100% humidity before plunge-freezing into liquid ethane
147 using a Vitrobot (CBRS, UT Austin). The vitreous sample grids were observed on a Glacios
148 microscope (Thermo Fisher) and images were captured at 200 kV with a 1.97 $Å^2$/pixel Falcon 4

149 camera. Data were collected using SerialEM version 3.9.0 beta and motion corrected using
150 cryoSPARC with 60 frames.
151

152 **Library Preparation, Sequencing, and Quality Control**

153 Library preparation was performed at the University of Texas Genomic Sequencing
154 Facility (GSAF) using the NEBNext Small RNA library preparation kit (E7330, New England
155 Biolabs) as previously published [50]. Samples were prepared with 14 cycles of PCR and the final
156 product was size selected using a 3% gel cassette on the Blue Pippin instrument (Sage Sciences),
157 with the parameters set to 105-165 bp. Final size selected libraries were checked for quality on
158 the Agilent BioAnalyzer with High Sensitivity DNA analysis kit (5067-4626, Agilent) to confirm
159 proper size selection. The Kapa Library Quantification kit for Illumina libraries (KK4602) was
160 used to determine the loading concentrations prior to sequencing. Samples were sequenced on a
161 NovaSeq 6000 Single Read, SR50 run, with read counts ranging from 25 to 32 million per sample.
162 The raw sequence data is publicly accessible (GSA: CRA008039).
163

164 **Analysis Pipeline**

165 Raw RNA reads were first passed through quality control (FastQC) and checked for read
166 quality and size distribution, which showed excellent average read quality (avg. PHRED > 36) and
167 expected read length (50 bp). The raw reads were trimmed for Illumina adaptors (QuasR,
168 BioConductor) and again passed through quality control (FastQC) to determine per base read
169 quality and size distribution, which again showed excellent average read quality (avg. PHRED >
170 36) and an expected read length distribution (~30 nt) based on electrophoresis performed before
171 library prep. The trimmed reads were aligned (RBowtie, Bioconductor) to the unmasked rat
172 genome (Rnor v6) with strict matching parameters to ensure reads were aligned to best-hit
173 locations but were allowed multiple mapping locations (n = 12) due to the promiscuous nature of
174 small RNA origins. If the alignment parameters were met but a read mapped to multiple locations,

175 the read was randomly assigned to one of the similar best hit locations. Alignment efficiency was
176 analyzed for cross-species contamination or PCR primer amplification artifacts and was found to
177 be highly efficient (~85%). The aligned reads were assigned a feature annotation (Seqmonk, R,
178 BioConductor), visualized, and analyzed for read count and length distribution. Our annotation
179 pipeline considered reads aligned to miRNA, piRNA, rRNA, snoRNA, snRNA, tRNA, long non-
180 coding RNA (lncRNA), vault RNA, and Y RNA. CpG islands were inadvertently included in the
181 pipeline, although at the time we did not have any expectation of finding sncRNAs aligned with
182 this category. We also obtained annotation tracks for nested and simple repeats (UCSC genome
183 database) and microsatellites (UCSC genome database). Reads were assigned an annotation
184 designation only after considering all other annotation types co-occurring in the same region.

185

186 **RESULTS**

187 **The size distribution of rat caput epididymosomes**

188 Particle tracking (NanoSight 300, Malvern Panalytical, Malvern, UK) was used to
189 determine the size distribution of the extracellular particles isolated from the caput of the rat
190 epididymis using the Qiagen exoEasy Maxi kit as described above. The isolated EPs from two
191 separate samples were analyzed 5 times each. The first sample had a mean EP size of 181.4 nm
192 (standard error [SE] 3), mode of 152 nm (SE 2.5), and standard deviation of 40.6 nm (SE 1.1) and
193 the second a mean of 178.7 (SE 0.5), mode of 156.1 (SE 3.8), and standard deviation of 45.7 nm
194 (SE 1.8). The size distribution and density of the extracellular particles analyzed are shown in
195 **Figure 1**. Approximately ~93% of all particles tracked were between 50 and 250 nm in size, which
196 are characteristic of epididymosomes [4].

197

198 **The morphology of rat caput EPs**

199 TEM and cryo-EM were used to determine the morphology of the extracellular particles
200 isolated from the caput of the rat epididymis using the Qiagen exoEasy Maxi kit as described
201 above. To increase the concentration of vesicles present in the sample for imaging, the epididymis
202 was thoroughly minced with scissors, and caput biofluid was collected by squeezing the tissue
203 with forceps. The isolated EPs from two separate samples were imaged using either TEM or cryo-
204 EM. TEM allowed us to visualize the composition of the sample, whereas cryo-EM aided in
205 visualization of EVs, including lipid bilayers and internal structures. Both types of samples were
206 composed of a population of intact round particles that possess a clear lipid bilayer/membrane,
207 which is characteristic of extracellular vesicles. Single, double, and multilayer vesicles,
208 characteristic of EV preparations and defined by the presence of one, two, or multiple membranes,
209 respectively, are presented in **Figure 2**. Cryo-EM imaging revealed clear lipid bilayer membranes
210 (**Figure 2C, D)**.

211

212 **The small RNA contents of rat caput EPs**

213 The sncRNA contents of rat epididymosomes were dominated by reads that aligned to
214 tRNA (79.1%) or piRNA loci (18.1% - **Figure 3A; Tables 1 & 2**). We were surprised at the
215 relatively low abundance of miRNA in rats considering that mice caput EVs primarily consist of
216 miRNA (~60% -- [20,29,34,35]). All other annotation types, including miRNAs, accounted for the
217 remaining 2.8% of the aligned reads. When tRNA and piRNA reads were removed from analysis
218 and aligned reads were analyzed as a proportion of the remaining reads (**Figure 3B**), the largest
219 remaining category belonged to reads that aligned to CpG islands (55.2%), which is not a known
220 unit of sncRNA expression (discussed below). The remaining reads aligned to Y RNA (24.6%),
221 lncRNA (7.5%), miRNA (6.4%), rRNA (4.3%), and snoRNA (1.8%).

222 We analyzed the length of the reads aligned and assigned to each respective sncRNA
223 category to determine if our annotation pipeline performed well and to describe the subspecies of
224 various sncRNAs (**Table 1**). Notably, there was strong consistency in profiles among the six
225 individual male rats (**Table 2**). The two canonical categories with known read lengths were
226 checked first (miRNA and piRNA) and are discussed next.

227

228 **Few miRNAs are loaded into rat caput EPs compared to mice**

229 The average read length for miRNA (22 nt) was exactly as expected [51,52] and showed a
230 90-percentile range of 19 – 27 nt (**Figure 3**). They account for only 0.18% of all reads. By contrast,
231 miRNAs account for ~60% of caput EVs in mice [34]. We set a cut-off of 10 reads per million
232 (RPM) to determine which miRNA were loaded into caput EPs and identified 15 miRNAs, ten of
233 which have previously been shown to exist either in sperm or EVs in various models, and five of
234 which are uncharacterized miRNAs (**Table 3**). This is a far fewer number than those in mouse EVs
235 (~350) using a similar threshold [20]. Of the 15 miRNAs identified in rat, 7 overlapped with those
236 reported in mice (miR-143, let-7c, let-7i, miR-26a, miR-99a, miR-143, miR-148 [20]). The most
237 abundant miRNA we identified in rats, miR-184, did not meet the threshold for abundance in mice
238 [20]. MiR-143, which is a hallmark of EVs in mice [20] and humans [34], was also found in rat
239 caput EVs.

240

241 **piRNAs are abundant and coincide with 5' tRNA fragments**

242 The average read length for piRNA was also as expected (30 nt; [52]) with a 90-percentile
243 range of 26 – 32 nt (**Figure 3**). We identified 81 piRNA loci that were substantially (> 10 RPM)
244 expressed across the genome, with clusters on chromosome 1, 2, 10, 13, 14 and 17. piRNAs
245 represented a substantial proportion (18.1%) of EPs in the rat caput epididymis. This is contrary
246 to what is found in mouse models (< 0.05%; [34,35]) but not entirely unexpected as rat pachytene

247 sperm are densely populated with piRNAs [53] depending on the stage of development [54,55]
248 presumably to control the expression of transposable elements in the germline [56] by directing
249 the catalyzation of *de novo* DNA methylation to suppress their expression [57]. The reasons for
250 this discrepancy between rats and mice could be due to a number of reasons. First, this may
251 represent a fundamental difference in the reproductive biology between the two species. Second,
252 it may be because the piRNAs that do exist in mouse caput EVs are typically categorized as tRNA-
253 halves instead of piRNA. We found that approximately 60% (49/81) of the expressed piRNA loci
254 overlapped with known tRNA loci; these accounted for a significant portion of all piRNA
255 annotated reads (82.3%). These are a known subclass of piRNAs termed tRNA-derived piRNA
256 (td-piRNAs; [58]) so we further analyzed their origin and determined that virtually all of these
257 reads aligned with the 5' end of tRNA loci (98.98%). tRNA derived-piRNA (td-piRNA) have been
258 described in the testes of marmosets where Piwi proteins were found to bind reads mapping to the
259 5'-tRNA^{Glu}, 5'-tRNA^{Gly}, and 5'-tRNA^{Val} loci [59]. Therefore, we categorized the tRNA type from
260 which piRNAs were generated and determined that the majority were derived from either 5'-
261 tRNA^{Gly} (53.3%) or 5'-tRNA^{Glu} (32.6%) loci; 5'-tRNA^{Lys} (8.5%) and 5'-tRNA^{Val} (2.3%)
262 originating reads were also identified. It is intriguing that these three identified td-piRNAs account
263 for three of the four td-piRNAs found here. To our knowledge this is the first evidence that td-
264 piRNA are in a position poised to be delivered to sperm in the epididymis via EVs. Additionally,
265 we append 5'-tRNA^{Lys}, the third most abundant td-piRNA in our analysis, as a potentially
266 significant td-piRNA in rats.

267

268 **tRNA fragments (tRFs) dominate the cargo of rat caput EPs**

269 We then analyzed other sncRNA categories where read lengths can be variable depending
270 on how the RNA is processed. In mouse models, nascent sperm in the caput contain few tRFs but
271 their abundance gradually increases as sperm transit to the cauda [22,60], a pattern that is mirrored
272 by the EVs found in the same epididymal compartment [34]. By comparison, reads from tRNA

273 loci dominated the cargo in our rat caput EPs (~79%). The reads aligned to tRNAs had an average
274 read length of 30 nt and a 90-percentile range of 28 – 31 nt (**Table 1**), suggesting that they are
275 either tRNA fragments (tRFs) or tRNA-halves, which are 14 – 30 nt and 30 – 40 nt in length,
276 respectively [61].

277 We further categorized tRNA reads by aligning them to either the 5' or 3' end of a given
278 tRNA locus and discovered that 99.35% of all reads aligned to the 5' end (**Figure 4A**). There are
279 two possible explanations for the overrepresentation of 5'-tRFs. First, rat caput EPs may be
280 selectively loaded with 5'-tRF fragments; these have actions similar to RNA interference as
281 governed by miRNAs, which act through the Argonaute pathway [62] to silence endogenous
282 retroelements in embryonic stem cells and embryos [22]. Alternatively, our observation may be
283 due to a technical bias in the sequencing library preparation procedure [61]. Libraries are amplified
284 with PCR during preparation, which can be prematurely aborted if an RNA molecule contains
285 modified tRNA nucleobases that would be too short for sequencing, thereby excluded, and not
286 detected during analysis. In order to confirm the dominating presence of 5'-tRFs in rat caput EPs,
287 a specific analysis pipeline (streamlined platform for observing tRNA – SPOt) would need to be
288 used to prevent observation bias [63].

289 Given their size distribution, we were able to further categorize the 5'-tRFs reads, which
290 show a 28 – 30 nt size distribution indictive of tRF-5c fragments, the longest of the three known
291 5'-tRFs, or tRNA-halves [64]. Alignment of reads to the tRNA structure (tRNAvis) confirmed
292 their identity as tRF-5c fragments because reads did not align to the anti-codon stem loop, which
293 would be characteristic of 5' tRNA-halves [61]. Because of the significant overlap of reads
294 identified between piRNAs and tRNA loci (presented above), we analyzed the proportion of tRNA
295 reads that could be accounted for by piRNA loci. We found that the majority of tRNA reads
296 (~81%) were unique to tRNAs and could not be accounted for by overlapping piRNA loci.

297 Finally, we analyzed the amino-acid feature that tRNA reads were derived from and found
298 that there was an over-representation of reads derived from Glycine-tRNAs (81.4%). Reads were
299 also found to originate from glutamate (7.7%), histidine (6.9%), and lysine (1.7%) tRNA loci

300 across the genome (**Figure 4B**). Finally, the size distribution for 3' tRNA reads (**Figure 4C**) was
301 similar to 5' tRNA reads (**Figure 4D**).
302
303 **rRNA fragments are present in three distinct lengths**
304 rRNA fragments (rRFs) have long been considered RNA degradation or apoptotic by-
305 products and are generally disregarded for any functional value. Compared to miRNA, piRNA,
306 and tRFs, little is known about the function or categories of rRFs and they have only recently been
307 described [65] with nearly no information existing in rats that we could find. Interestingly, rRFs
308 appear in immunoprecipitations with the Argonaute complex in mice and humans, which suggests
309 a role for translational regulation [66]. In humans, three distinct categories of rRFs are known with
310 differential expression in each of the rRNA categories (i.e., 5s, 5.8s, 18s, and 28s): short (18-21
311 nt), intermediate (24-25 nt), and long (26-33 nt) [65].
312 Here, we identify the presence of rRFs in rat caput EPs. Reads aligned to rRNA loci had
313 an average length of 22 nt and a broad 90-percentile range of 17 – 31 nt (**Table 1**). rRNA is
314 expressed as a 45s pre-rRNA, which contains the transcripts for 18s, 5.8s, and 28s rRNA,
315 organized as cassettes of tandem repeats on the short arms of chromosomes 3, 11, and 12 of the
316 rat genome [67]. The rat reference genomes are poorly annotated for these repeating cassettes
317 because the number of repeats often varies between individuals. Hence, these regions are typically
318 masked in alignment reference genomes. Nonetheless, there are a number of 5s rRNAs, which are
319 expressed separately from the 45s pre-rRNA, and 5.8s rRNA loci that are annotated in the rat
320 reference genome that we analyzed. Approximately 80% of rRNA derived reads aligned to 5.8s
321 loci (**Figure 5A**). Subcategories of rRFs have been described from human samples where short
322 (18-19 nt), intermediate (24-25 nt), and long (32-33 nt) rRFs are expressed depending on the rRNA
323 type (e.g. 5s vs 5.8s) [65]. Our data generally fit the categories described in human samples: 5s
324 rRNA resulted in either short or long transcripts (**Figure 5B**) whereas 5.8s rRNA resulted in
325 intermediate fragments (**Figure 5C**). rRFs are sparsely reported in reproductive tissue (Humans,

326 [68,69]; Bovine, [70]). We believe this is the first report of their presence in caput EP samples,
327 meriting future studies on a role for rRFs in reproduction.

328

329 **Fragments of other RNA types are also present in rat caput EPs**

330 Finally, we observed that the Y RNA was present in caput EPs at levels ~4 times that of
331 miRNA, which is surprising because we are not aware of any reports of Y RNA in epididymal
332 EVs, although they are found in EVs of other tissue types [71–73]. Full length Y RNAs are ~80 –
333 110 nt in length [74]. We identified 13 (of 28) Y RNA loci with substantial expression (> 10 reads
334 per kilobase million – RPKM). These reads demonstrated a sharp peak at 31 nt and a smaller peak
335 at 22 nt with a 90-percentile range of 22 – 31 nt (**Table 1**). These results suggest that rat caput EVs
336 include fragments of Y RNA as a part of their sncRNA repertoire.

337

338 **Small RNA molecules are expressed from within CpG islands**

339 We identified dense clusters of expression that appeared to be contained within the
340 boundaries of GC-rich CpG islands (**Figure 6A**). CpG islands are typically annotated based on
341 sequence characteristics defined as longer than 200-bp with a GC content higher than 50% and an
342 expected-to-observed ratio greater than 0.6 [75]. Many of the first CpG islands were identified at
343 the 5' end of "housekeeping" genes [76,77] but have since been computationally and
344 experimentally predicted across the genome, including in inter- and intragenic space [78]. Parts of
345 CpG islands are sometimes transcribed on the 5' or 3' end of expressed genes and removed during
346 splicing unless they extend into an exon, including within sncRNAs [78,79]. Because small RNAs
347 have not previously been ascribed to the boundaries of CpG islands, we meticulously characterized
348 these features, and further challenged this result by trying to ascribe reads contained with CpG
349 islands to other surrounding or overlying genomic features.

350 In total we identified 50 CpG islands with significant expression (>10 RPKM) of small
351 RNA molecules. We inspected the distribution of reads (SeqMonk) within each of these CpG
352 islands and were able to rule out the majority of them due to overlapping features that had
353 canonical expression patterns expected from features like rRNA and piRNA (**Figure 6B**) or tRNA
354 (**Figure 5C**). These loci were removed from further analyses and the remaining 12 CpG islands
355 were treated as an annotation category for sncRNAs. We found this category to be the third most
356 abundant behind tRNA and piRNA reads (**Figure 3A** and **B**), and that the reads derived from CpG
357 islands had a length distribution pattern that was distinct from all of the other analyzed categories
358 (**Figure 3C**) with a median length of 19 nt and a 90-percentile range of 15 – 28 nt (**Table 1**). As
359 expected, the GC content of reads aligned to CpG islands was substantial (~78%) compared to the
360 average of all aligned reads (~50%).

361 We calculated a signal-to-noise (s/n) ratio to determine if the reads we observed within
362 CpG islands were due to random chance [65]. When compared to the number of reads per kilobase
363 million (RPKM) over a 10 kb rolling window across the entire genome, our identified CpG islands
364 had a 609 s/n ratio. When compared to all CpG islands across the entire genome, our identified
365 CpG islands had a 92 s/n ratio. Put simply, the reads contained within the identified CpG islands
366 were 609 times more abundant than a random 10kb window in the genome and 92 times more
367 abundant than an average CpG island, indicating that the reads we observed were very unlikely to
368 be due to random chance.

369 Because CpG islands are not known units of small RNA expression, we then systematically
370 considered whether the observed reads were due to other overlying features. We observed that
371 those CpG islands that contained more piRNA loci appeared to be associated with more reads
372 (**Figure 7A**). The function of piRNA is RNA-guided silencing of transposable elements,
373 particularly in the germline before exit from the testis [54,80–82]. Hence, the presence of piRNA
374 in caput EVs would not be surprising. However, because the read distribution we identified for
375 other piRNA loci (e.g. **Figure 6B**) was very different from reads identified for CpG islands (e.g.
376 **Figure 6A**) we considered that the transcripts we were observing might be secondary piRNAs

377 generated via the ping-pong cycle wherein piRNAs are amplified by binding expressed mobile
378 elements [54,83] or byproducts from their generation [84–86]. We therefore analyzed the
379 relationship between piRNA loci and the reads expressed within CpG islands; when normalized
380 for the read depth and length of the CpG island (RPKM) the relationship was virtually non-existent
381 (R^2 = 0.077, **Table 4**). We quantified the reads that aligned under known piRNA loci and found
382 that ~48% of the total reads within the boundaries of CpG islands were also associated with piRNA
383 loci. However, we are hesitant to classify these reads as piRNA because they do not follow the
384 canonical length distribution associated with primary or secondary piRNA (~30nt) identified here
385 and as reported elsewhere [87].

386 The byproducts of secondary piRNA generation are typically ~19-nt, which matches the
387 length distribution we see here. We consider this the most likely possibility of those considered,
388 but our observation does not fully match their description. First, a subset of the CpG islands that
389 we identified were not associated with any known piRNA annotations. Second, the mechanism by
390 which piRNA biproducts are generated usually results in 19-nt RNA from both strands and broad
391 areas that are only constrained by the targets that primary and secondary piRNA bind. We therefore
392 analyzed the source strand of the identified reads and found they are almost exclusively expressed
393 from a single strand in the orientation of the primary piRNA annotations in the instances there
394 were any at all (**Table 4**). Third, we looked at overlying repeat elements (LINE, SINE, and LTRs)
395 and found these CpG islands void of any such annotated repeats. Because piRNA and tRNA are
396 often associated, we also analyzed the proportion of reads aligning to tRNA loci and found none
397 of the reads (0%) within CpG islands were expressed from known tRNA loci. In a subset of the
398 CpG islands we observed, there was an abundance of predicted (eponine) transcriptional start sites
399 (**Figure 7B**), but this was not always the case (e.g. **Figure 6A**).

400 Finally, half (6/12) of the identified CpG islands were associated with annotated 5.8s rRNA
401 loci (**Table 4**). None of the CpG islands we identified were in proximity to known locations of
402 rRNA cassettes, namely, on the short arms of chromosomes 3, 11, and 12 [67]. Notwithstanding,
403 the rat genome is poorly annotated for rRNA, so to overcome this shortcoming in the available

404 annotations we used BLAST to align the raw sequences expressed from CpG islands to the
405 available rat rRNA sequences: 45s, 32s (which includes the 28s rRNA and 5' sequence between
406 the transcription start site and 28s), 28s, 18s, and 5.8s. Approximately one third (~34.3%) of all
407 reads derived from CpG islands aligned to some form of rRNA or precursor rRNA. Of those reads
408 that aligned to any form of rRNA, the vast majority were derived from the 28s sequence (86.1%),
409 while the 18s (11.15%), and 5.8s (0.16%) accounted for a small proportion of the reads. The
410 remaining reads (2.6%) aligned to the external or internal transcribed spacers within the full length
411 45s rRNA precursor transcript. Given the proximity of these reads to apparent rRNA cassettes, we
412 cannot rule out that some portion of the observed CpG islands may be a part of the ~30 kb non-
413 transcribed spacer that separates 45s repeats. But, as the name implies, these portions are up or
414 downstream of rRNA and should not be transcribed.

415 In summary, while it appears that the CpG islands we identified as expressing 19 nt small
416 RNAs were in the vicinity of heretofore unannotated rRNA or piRNA loci, the reads observed
417 expressed within CpG islands cannot be fully accounted for by either of these designations nor are
418 their expression profiles congruent. Therefore, we believe this is a novel category of small RNA
419 that warrants additional investigation.

420

421 **DISCUSSION**

422 Epididymosomes from the caput are an essential component of sperm maturation
423 and acquisition of function [5,88,89]. The proteins transferred to sperm via caput EVs are believed
424 to assist in sperm-zona binding [16] and the development of motility in sperm [90]. Caput EVs are
425 also implicated in the control of heritable non-genetic phenotypes, as their sncRNA cargo is altered
426 by stress [22,26,29], diet [27,30,91], and alcohol consumption [31]. Thus, caput EVs and their
427 contents play roles in development and the health and behavior of offspring. Support for the role
428 of sncRNA in transgenerational inheritance is bolstered by experiments in which they are directly

429 injected into zygotes or sperm [32]. This method has been used to demonstrate inter- or
430 transgenerational inheritance of metabolic [27,30,92] and behavioral phenotypes [93–95].

431 Here, we provide the first comprehensive characterization of small RNAs derived from
432 caput EPs in the rat, and demonstrate quantitative and qualitative aspects unique to this species.
433 EPs isolated from the caput epididymis match the size range of epididymosomes and their small
434 RNA contents are dominated by tRFs and piRNA, containing far fewer miRNAs than expected
435 from other organisms (Mice, [29,34,35]; Humans, [96]). We also identify Y RNA fragments in
436 caput EPs for the first time in any organism, although they are expressed in EVs of other organs
437 [71–73]. Finally, we identify a potentially novel small RNA molecule that is expressed from GC-
438 rich CpG islands that cannot be accounted for by known overlying small RNA features, and which
439 have a unique size distribution that is distinct from other small RNAs analyzed.

440 The small RNA contents of EVs from the mouse caput epididymis are primarily miRNAs
441 (~60% - [29,34,35]), with over 350 expressed [20]. This is in contrast to the rat in which miRNAs
442 were a small portion (0.18%) of the small RNA complement. There were also substantial species
443 differences in tRFs, which are the second most abundant category (~30%) in mouse caput EVs
444 while piRNAs are present at very low levels in mice (<0.05% - [34,35]). Here, we show in rats
445 that tRFs are by far the most abundant category (~79%) and piRNAs are second most abundant
446 (~18%). Further work is needed to validate these findings and to understand why there are these
447 dramatic species differences in the EV sncRNA cargo.

448 Finally, we believe we have discovered a novel type of small RNA that is expressed from
449 within the boundaries of CpG islands. Based on the analyses we performed and the data presented
450 here, we do not believe that alternative sncRNAs (rRNA fragments, piRNAs, or piRNA
451 amplification byproducts) can account for these 19-nt small RNAs. More specifically, these "CpG
452 island small RNAs" extend outside of the boundaries of annotated rRNA and piRNA, which
453 account for only a portion of the observations, and do not abide by their respective canonical length
454 characteristics. It is possible that these observations could be the 19mer byproduct of piRNA
455 amplification observed elsewhere [84–86] but there are 3 reasons we do not think this is likely.

456 First, we observe these reads in EPs while the byproducts of piRNA amplification have only been
457 found to exist in pre-pachytene spermatocytes and should be derived from both the sense and anti-
458 sense strands, a characteristic we do not see. If this observation is due to 19mer piRNA
459 amplification byproducts generated in the epididymis instead of spermatocytes themselves, our
460 data would suggest that secondary piRNA are produced in the epididymis and they, along with
461 their byproducts, are actively transported to spermatozoa transiting the epididymis. Second, the
462 reads we observe are expressly within the boundaries of CpG islands with a GC content not
463 reported elsewhere. The specificity of the expression loci, and the lack of a high GC content in
464 other reports on the production of secondary piRNA make their identity as byproducts unlikely.
465 Finally, we observe expression from multiple CpG islands not linked with known piRNA loci. If
466 these are indeed the byproduct of piRNA amplification, our data would represent the identification
467 of novel piRNA loci that would seem to be important for the final steps of sperm maturation.
468 Mature sperm transiting the epididymis should be transcriptionally quiescent [97–100], and
469 therefore transposons, which are the presumed target of piRNA, should not be expressed.
470 Ascertaining a functional role of these small RNAs requires further investigation.

471 In summary, EPs from the rat caput epididymis carry a complex repertoire of small RNAs
472 and their contents are substantially different from the mouse. The dominant features we identify
473 are tRNA fragments and piRNAs derived from tRNA loci. MicroRNAs are poorly represented in
474 stark contrast to mice. We also report the presence of two known types of small RNA not
475 previously seen in caput EVs, rRNA fragments and Y RNA fragments, and identify a potentially
476 novel small RNA we have termed CpG island (CpGi) sRNAs. Considering that epididymal EVs
477 can transfer their RNA cargo to sperm, these data represent an exciting collection of possibilities
478 for future research on mechanisms of basic reproductive biology and the complexities of epigenetic
479 transgenerational inheritance.

480

481 **Acknowledgement:** The authors recognize Mandee Bell and Lindsay M. Thompson for their
482 assistance with animal husbandry, treatment, and sample collection. We thank Michelle Mikesh

483 for her assistance in the use of transmission electron microscopy, and Dr. Axel Brilot and Dr. Evan
484 Schwartz for their assistance in the use of cryo-electron microscopy. We also acknowledge the
485 excellent work (small RNA library preparation and sequencing) performed by the Genomic
486 Sequencing and Analysis Facility at UT Austin, Center for Biomedical Research Support. RRID#:
487 SCR_021713. Finally, we would like to thank Dr. Nicholas Peppas and his laboratory for training,
488 guidance, and execution of particle tracking analysis and Dr. Blerta Xhemalce for reviewing our
489 approach and data.
490
491 **Grant funding**: Supported by R35 ES035024 and R21 ES034067 to A.C.G., and PhRMA
492 Foundation Postdoctoral Fellowship to R.G.
493
494 **Conflict of Interest:** The authors declare no conflict of interest.
495 **Data Availability:** The raw sequence data reported in this paper have been deposited in the
496 Genome Sequence Archive [101] at the National Genomics Data Center [102] that is publicly
497 accessible at https://ngdc.cncb.ac.cn/gsa accession GSA: CRA008039.
498 **ARRIVE:** The study was carried out according to the ARRIVE guidelines [41].

499 **REFERENCES**
500

501 1. Hermo, L.; Pelletier, R. -Marc; Cyr, D.G.; Smith, C.E. Surfing the Wave, Cycle, Life History,
502 and Genes/Proteins Expressed by Testicular Germ Cells. Part 1: Background to
503 Spermatogenesis, Spermatogonia, and Spermatocytes. *Microsc Res Techniq* 2010, *73*, 241–278,
504 doi:10.1002/jemt.20783.

505 2. Cornwall, G.A. New Insights into Epididymal Biology and Function. *Hum Reprod Update*
506 2009, *15*, 213–227, doi:10.1093/humupd/dmn055.

507 3. Sullivan, R.; Saez, F. Epididymosomes, Prostasomes, and Liposomes: Their Roles in
508 Mammalian Male Reproductive Physiology. *Reproduction* 2001, *146*, R21–R35,
509 doi:10.1530/rep-13-0058.

510 4. Sullivan, R. Epididymosomes: A Heterogeneous Population of Microvesicles with Multiple
511 Functions in Sperm Maturation and Storage. *Asian J Androl* 2015, *0*, 0, doi:10.4103/1008-
512 682x.155255.

513 5. Martin-DeLeon, P.A. Epididymosomes: Transfer of Fertility-Modulating Proteins to the
514 Sperm Surface. *Asian J Androl* 2015, *17*, 720–725, doi:10.4103/1008-682x.155538.

515 6. Martin-DeLeon, P.A. Epididymal SPAM1 and Its Impact on Sperm Function. *Mol Cell*
516 *Endocrinol* 2006, *250*, 114–121, doi:10.1016/j.mce.2005.12.033.

517 7. Fornés, M.W.; Barbieri, A.; Cavicchia, J.C. Morphological and Enzymatic Study of
518 Membrane-bound Vesicles from the Lumen of the Rat Epididymis. *Andrologia* 1995, *27*, 1–5,
519 doi:10.1111/j.1439-0272.1995.tb02087.x.

520 8. Rejraji, H.; Sion, B.; Prensier, G.; Carreras, M.; Motta, C.; Frenoux, J.-M.; Vericel, E.;
521 Grizard, G.; Vernet, P.; Drevet, J.R. Lipid Remodeling of Murine Epididymosomes and
522 Spermatozoa During Epididymal Maturation. *Biol Reprod* 2006, *74*, 1104–1113,
523 doi:10.1095/biolreprod.105.049304.

524 9. Grimalt, P.; Bertini, F.; Fornes, M.W. High-Affinity Sites for Beta-D-Galactosidase on
525 Membrane-Bound Vesicles Isolated from Rat Epididymal Fluid. *Arch Andrology* 2009, *44*, 85–
526 91, doi:10.1080/014850100262245.

527 10. Hermo, L.; Jacks, D. Nature's Ingenuity: Bypassing the Classical Secretory Route via
528 Apocrine Secretion. *Mol Reprod Dev* 2002, *63*, 394–410, doi:10.1002/mrd.90023.

529 11. Oh, J.S.; Han, C.; Cho, C. ADAM7 Is Associated with Epididymosomes and Integrated into
530 Sperm Plasma Membrane. *Mol Cells* 2009, *28*, 441–446, doi:10.1007/s10059-009-0140-x.

531 12. Zhou, W.; Iuliis, G.N.D.; Dun, M.D.; Nixon, B. Characteristics of the Epididymal Luminal
532 Environment Responsible for Sperm Maturation and Storage. *Front Endocrinol* 2018, *9*, 59,
533 doi:10.3389/fendo.2018.00059.

534 13. Frenette, G.; Lessard, C.; Sullivan, R. Polyol Pathway along the Bovine Epididymis. *Mol*
535 *Reprod Dev* 2004, *69*, 448–456, doi:10.1002/mrd.20170.

536 14. Sutovsky, P.; Moreno, R.; Ramalho-Santos, J.; Dominko, T.; Thompson, W.E.; Schatten, G.
537 A Putative, Ubiquitin-Dependent Mechanism for the Recognition and Elimination of Defective
538 Spermatozoa in the Mammalian Epididymis. *J Cell Sci* 2001, *114*, 1665–1675,
539 doi:10.1242/jcs.114.9.1665.

540 15. D'Amours, O.; Frenette, G.; Bordeleau, L.-J.; Allard, N.; Leclerc, P.; Blondin, P.; Sullivan,
541 R. Epididymosomes Transfer Epididymal Sperm Binding Protein 1 (ELSPBP1) to Dead
542 Spermatozoa During Epididymal Transit in Bovine1. *Biol Reprod* 2012, *87*, Article 94, 1-11,
543 doi:10.1095/biolreprod.112.100990.

544 16. Nixon, B.; Iuliis, G.N.D.; Hart, H.M.; Zhou, W.; Mathe, A.; Bernstein, I.R.; Anderson, A.L.;
545 Stanger, S.J.; Skerrett-Byrne, D.A.; Jamaluddin, M.F.B.; et al. Proteomic Profiling of Mouse
546 Epididymosomes Reveals Their Contributions to Post-Testicular Sperm Maturation. *Mol Cell*
547 *Proteomics* 2019, *18*, S91–S108, doi:10.1074/mcp.ra118.000946.

548 17. Girouard, J.; Frenette, G.; Sullivan, R. Comparative Proteome and Lipid Profiles of Bovine
549 Epididymosomes Collected in the Intraluminal Compartment of the Caput and Cauda
550 Epididymidis. *Int J Androl* 2011, *34*, e475–e486, doi:10.1111/j.1365-2605.2011.01203.x.

551 18. Kalluri, R.; LeBleu, V.S. The Biology, Function, and Biomedical Applications of Exosomes.
552 *Science* 2020, *367*, doi:10.1126/science.aau6977.

553 19. Belleanne, C.; Calvo, zequiel; Caballero, J.; Sullivan, R. Epididymosomes Convey Different
554 Repertoires of MicroRNAs Throughout the Bovine Epididymis1. *Biol Reprod* 2013, *89*, Article
555 30, 1-11, doi:10.1095/biolreprod.113.110486.

556 20. Reilly, J.N.; McLaughlin, E.A.; Stanger, S.J.; Anderson, A.L.; Hutcheon, K.; Church, K.;
557 Mihalas, B.P.; Tyagi, S.; Holt, J.E.; Eamens, A.L.; et al. Characterisation of Mouse
558 Epididymosomes Reveals a Complex Profile of MicroRNAs and a Potential Mechanism for
559 Modification of the Sperm Epigenome. *Sci Rep-uk* 2016, *6*, 31794, doi:10.1038/srep31794.

560 21. Caballero, J.N.; Frenette, G.; Belleannée, C.; Sullivan, R. CD9-Positive Microvesicles
561 Mediate the Transfer of Molecules to Bovine Spermatozoa during Epididymal Maturation. *Plos*
562 *One* 2013, *8*, e65364, doi:10.1371/journal.pone.0065364.

563 22. Sharma, U.; Conine, C.C.; Shea, J.M.; Boskovic, A.; Derr, A.G.; Bing, X.Y.; Belleannee, C.;
564 Kucukural, A.; Serra, R.W.; Sun, F.; et al. Biogenesis and Function of TRNA Fragments during
565 Sperm Maturation and Fertilization in Mammals. *Science* 2016, *351*, 391,
566 doi:10.1126/science.aad6780.

567 23. Conine, C.C.; Sun, F.; Song, L.; Rivera-Pérez, J.A.; Rando, O.J. Small RNAs Gained during
568 Epididymal Transit of Sperm Are Essential for Embryonic Development in Mice. *Dev Cell* 2018,
569 *46*, 470-480.e3, doi:10.1016/j.devcel.2018.06.024.

570 24. Gapp, K.; Jawaid, A.; Sarkies, P.; Bohacek, J.; Pelczar, P.; Prados, J.; Farinelli, L.; Miska, E.;
571 Mansuy, I.M. Implication of Sperm RNAs in Transgenerational Inheritance of the Effects of
572 Early Trauma in Mice. *Nat Neurosci* 2014, *17*, 667–669, doi:10.1038/nn.3695.

573 25. Suryawanshi, A.R.; Khan, S.A.; Joshi, C.S.; Khole, V.V. Epididymosome-Mediated
574 Acquisition of MMSDH, an Androgen-Dependent and Developmentally Regulated Epididymal
575 Sperm Protein. *J Androl* 2012, *33*, 963–974, doi:10.2164/jandrol.111.014753.

576 26. Rodgers, A.B.; Morgan, C.P.; Bronson, S.L.; Revello, S.; Bale, T.L. Paternal Stress Exposure
577 Alters Sperm MicroRNA Content and Reprograms Offspring HPA Stress Axis Regulation. *J*
578 *Neurosci* 2013, *33*, 9003--9012, doi:10.1523/jneurosci.0914-13.2013.

579 27. Chen, Q.; Yan, M.; Cao, Z.; Li, X.; Zhang, Y.; Shi, J.; Feng, G.; Peng, H.; Zhang, X.; Zhang,
580 Y.; et al. Sperm TsRNAs Contribute to Intergenerational Inheritance of an Acquired Metabolic
581 Disorder. *Science* 2016, *351*, 397, doi:10.1126/science.aad7977.

582 28. Fullston, T.; Teague, E.M.C.O.; Palmer, N.O.; DeBlasio, M.J.; Mitchell, M.; Corbett, M.;
583 Print, C.G.; Owens, J.A.; Lane, M. Paternal Obesity Initiates Metabolic Disturbances in Two
584 Generations of Mice with Incomplete Penetrance to the F2 Generation and Alters the
585 Transcriptional Profile of Testis and Sperm MicroRNA Content. *Faseb J* 2013, *27*, 4226–4243,
586 doi:10.1096/fj.12-224048.

587 29. Short, A.; Fennell, K.; Perreau, V.; Fox, A.; O'Bryan, M.; Kim, J.H.; Bredy, T.; Pang, T.;
588 Hannan, A. Elevated Paternal Glucocorticoid Exposure Alters the Small Noncoding RNA Profile
589 in Sperm and Modifies Anxiety and Depressive Phenotypes in the Offspring. *Translational*
590 *Psychiatry* 2016, *6*.

591 30. Barbosa, T. de C.; Ingerslev, L.R.; Alm, P.S.; Versteyhe, S.; Massart, J.; Rasmussen, M.;
592 Donkin, I.; Sjögren, R.; Mudry, J.M.; Vetterli, L.; et al. High-Fat Diet Reprograms the
593 Epigenome of Rat Spermatozoa and Transgenerationally Affects Metabolism of the Offspring.
594 *Mol Metab* 2015, *5*, 184–197, doi:10.1016/j.molmet.2015.12.002.

595 31. Rompala, G.R.; Mounier, A.; Wolfe, C.M.; Lin, Q.; Lefterov, I.; Homanics, G.E. Heavy
596 Chronic Intermittent Ethanol Exposure Alters Small Noncoding RNAs in Mouse Sperm and
597 Epididymosomes. *Frontiers Genetics* 2018, *9*, 32–32, doi:10.3389/fgene.2018.00032.

598 32. Rassoulzadegan, M.; Grandjean, V.; Gounon, P.; Vincent, S.; Gillot, I.; Cuzin, F. RNA-
599 Mediated Non-Mendelian Inheritance of an Epigenetic Change in the Mouse. *Nature* 2006, *441*,
600 469–474, doi:10.1038/nature04674.

601 33. Chan, J.C.; Morgan, C.P.; Leu, N.A.; Shetty, A.; Cisse, Y.M.; Nugent, B.M.; Morrison, K.E.;
602 Jašarević, E.; Huang, W.; Kanyuch, N.; et al. Reproductive Tract Extracellular Vesicles Are

603 Sufficient to Transmit Intergenerational Stress and Program Neurodevelopment. *Nat Commun*
604 2020, *11*, 1499, doi:10.1038/s41467-020-15305-w.

605 34. Trigg, N.A.; Eamens, A.L.; Nixon, B. The Contribution of Epididymosomes to the Sperm
606 Small RNA Profile. *Reproduction* 2019, *1*, R209–R223, doi:10.1530/rep-18-0480.

607 35. Hutcheon, K.; McLaughlin, E.A.; Stanger, S.J.; Bernstein, I.R.; Dun, M.D.; Eamens, A.L.;
608 Nixon, B. Analysis of the Small Non-Protein-Coding RNA Profile of Mouse Spermatozoa
609 Reveals Specific Enrichment of PiRNAs within Mature Spermatozoa. *Rna Biol* 2017, *14*, 1776–
610 1790, doi:10.1080/15476286.2017.1356569.

611 36. Wei, H.; Zhou, B.; Zhang, F.; Tu, Y.; Hu, Y.; Zhang, B.; Zhai, Q. Profiling and Identification
612 of Small RDNA-Derived RNAs and Their Potential Biological Functions. *Plos One* 2013, *8*,
613 e56842, doi:10.1371/journal.pone.0056842.

614 37. Sipilä, P.; Björkgren, I. Segment-Specific Regulation of Epididymal Gene Expression.
615 *Reproduction* 2016, *152*, R91–R99, doi:10.1530/rep-15-0533.

616 38. Wei, Y.; Schatten, H.; Sun, Q.-Y. Environmental Epigenetic Inheritance through Gametes
617 and Implications for Human Reproduction. *Hum Reprod Update* 2015, *21*, 194–208,
618 doi:10.1093/humupd/dmu061.

619 39. Ellenbroek, B.; Youn, J. Rodent Models in Neuroscience Research: Is It a Rat Race? *Dis*
620 *Model Mech* 2016, *9*, 1079–1087, doi:10.1242/dmm.026120.

621 40. Burns, S.B.; Szyszkowicz, J.K.; Luheshi, G.N.; Lutz, P.-E.; Turecki, G. Plasticity of the
622 Epigenome during Early-Life Stress. *Semin Cell Dev Biol* 2018, *77*, 115–132,
623 doi:10.1016/j.semcdb.2017.09.033.

624 41. Sert, N.P. du; Ahluwalia, A.; Alam, S.; Avey, M.T.; Baker, M.; Browne, W.J.; Clark, A.;
625 Cuthill, I.C.; Dirnagl, U.; Emerson, M.; et al. Reporting Animal Research: Explanation and
626 Elaboration for the ARRIVE Guidelines 2.0. *Plos Biol* 2020, *18*, e3000411,
627 doi:10.1371/journal.pbio.3000411.

628 42. Goldman, J.M.; Murr, A.S.; Cooper, R.L. The Rodent Estrous Cycle: Characterization of
629 Vaginal Cytology and Its Utility in Toxicological Studies. *Birth Defects Res Part B Dev*
630 *Reproductive Toxicol* 2007, *80*, 84–97, doi:10.1002/bdrb.20106.

631 43. Hilz, E.N.; Lee, H.J. Estradiol and Progesterone in Female Reward-Learning, Addiction, and
632 Therapeutic Interventions. *Front Neuroendocrin* 2022, 101043,
633 doi:10.1016/j.yfrne.2022.101043.

634 44. Connor, K.; Ramamoorthy, K.; Moore, M.; Mustain, M.; Chen, I.; Safe, S.; Zacharewski, T.;
635 Gillesby, B.; Joyeux, A.; Balaguer, P. Hydroxylated Polychlorinated Biphenyls (PCBs) as
636 Estrogens and Antiestrogens: Structure-Activity Relationships. *Toxicol Appl Pharm* 1997, *145*,
637 111--123, doi:10.1006/taap.1997.8169.

638 45. Yuan, F.; Li, Y.-M.; Wang, Z. Preserving Extracellular Vesicles for Biomedical
639 Applications: Consideration of Storage Stability before and after Isolation. *Drug Deliv* 2021, *28*,
640 1501–1509, doi:10.1080/10717544.2021.1951896.

641 46. Gelibter, S.; Marostica, G.; Mandelli, A.; Siciliani, S.; Podini, P.; Finardi, A.; Furlan, R. The
642 Impact of Storage on Extracellular Vesicles: A Systematic Study. *J Extracell Vesicles* 2022, *11*,
643 e12162, doi:10.1002/jev2.12162.

644 47. Buschmann, D.; Kirchner, B.; Hermann, S.; Märte, M.; Wurmser, C.; Brandes, F.; Kotschote,
645 S.; Bonin, M.; Steinlein, O.K.; Pfaffl, M.W.; et al. Evaluation of Serum Extracellular Vesicle
646 Isolation Methods for Profiling MiRNAs by Next-generation Sequencing. *J Extracell Vesicles*
647 2018, *7*, 1481321, doi:10.1080/20013078.2018.1481321.

648 48. Musante, L.; Tataruch, D.; Gu, D.; Benito-Martin, A.; Calzaferri, G.; Aherne, S.; Holthofer,
649 H. A Simplified Method to Recover Urinary Vesicles for Clinical Applications and Sample
650 Banking. *Sci Rep-uk* 2014, *4*, 7532, doi:10.1038/srep07532.

651 49. Luo, X.; Jean-Toussaint, R.; Sacan, A.; Ajit, S.K. Differential RNA Packaging into Small
652 Extracellular Vesicles by Neurons and Astrocytes. *Cell Commun Signal* 2021, *19*, 75,
653 doi:10.1186/s12964-021-00757-4.

654 50. Herbert, Z.T.; Thimmapuram, J.; Xie, S.; Kershner, J.P.; Kolling, F.W.; Ringelberg, C.S.;
655 LeClerc, A.; Alekseyev, Y.O.; Fan, J.; Podnar, J.W.; et al. Multisite Evaluation of Next-
656 Generation Methods for Small RNA Quantification. *J Biomol Techniques Jbt* 2020, *31*, 47–56,
657 doi:10.7171/jbt.20-3102-001.

658 51. Ruvkun, G. Glimpses of a Tiny RNA World. *Science* 2001, *294*, 797–799,
659 doi:10.1126/science.1066315.

660 52. Marzec, M. Size Does Matter: PiRNA and MiRNA Targeting. *Trends Biochem Sci* 2021, *47*,
661 287–288, doi:10.1016/j.tibs.2021.12.001.

662 53. Stermer, A.R.; Reyes, G.; Hall, S.J.; Boekelheide, K. Small RNAs in Rat Sperm Are a
663 Predictive and Sensitive Biomarker of Exposure to the Testicular Toxicant Ethylene Glycol
664 Monomethyl Ether. *Toxicol Sci* 2019, *169*, 399–408, doi:10.1093/toxsci/kfz041.

665 54. Aravin, A.A.; Sachidanandam, R.; Girard, A.; Fejes-Toth, K.; Hannon, G.J. Developmentally
666 Regulated PiRNA Clusters Implicate MILI in Transposon Control. *Science* 2007, *316*, 744–747,
667 doi:10.1126/science.1142612.

668 55. Smorag, L.; Zheng, Y.; Nolte, J.; Zechner, U.; Engel, W.; Pantakani, D.V.K. MicroRNA
669 Signature in Various Cell Types of Mouse Spermatogenesis: Evidence for Stage-specifically
670 Expressed MiRNA-221, -203 and -34b-5p Mediated Spermatogenesis Regulation. *Biol Cell*
671 2012, *104*, 677–692, doi:10.1111/boc.201200014.

672 56. Newkirk, S.J.; Lee, S.; Grandi, F.C.; Gaysinskaya, V.; Rosser, J.M.; Berg, N.V.; Hogarth,
673 C.A.; Marchetto, M.C.N.; Muotri, A.R.; Griswold, M.D.; et al. Intact PiRNA Pathway Prevents
674 L1 Mobilization in Male Meiosis. *Proc National Acad Sci* 2017, *114*, E5635–E5644,
675 doi:10.1073/pnas.1701069114.

676 57. Peng, J.C.; Lin, H. Beyond Transposons: The Epigenetic and Somatic Functions of the Piwi-
677 PiRNA Mechanism. *Curr Opin Cell Biol* 2013, *25*, 190–194, doi:10.1016/j.ceb.2013.01.010.

678 58. Honda, S.; Kawamura, T.; Loher, P.; Morichika, K.; Rigoutsos, I.; Kirino, Y. The Biogenesis
679 Pathway of TRNA-Derived PiRNAs in Bombyx Germ Cells. *Nucleic Acids Res* 2017, *45*, 9108–
680 9120, doi:10.1093/nar/gkx537.

681 59. Hirano, T.; Iwasaki, Y.W.; Lin, Z.Y.-C.; Imamura, M.; Seki, N.M.; Sasaki, E.; Saito, K.;
682 Okano, H.; Siomi, M.C.; Siomi, H. Small RNA Profiling and Characterization of PiRNA
683 Clusters in the Adult Testes of the Common Marmoset, a Model Primate. *Rna* 2014, *20*, 1223–
684 1237, doi:10.1261/rna.045310.114.

685 60. Stanger, S.J.; Bernstein, I.R.; Anderson, A.L.; Hutcheon, K.; Dun, M.D.; Eamens, A.L.;
686 Nixon, B. The Abundance of a Transfer RNA-Derived RNA Fragment Small RNA
687 Subpopulation Is Enriched in Cauda Spermatozoa. *Exrna* 2020, *2*, 17, doi:10.1186/s41544-020-
688 00058-x.

689 61. Shen, Y.; Yu, X.; Zhu, L.; Li, T.; Yan, Z.; Guo, J. Transfer RNA-Derived Fragments and
690 TRNA Halves: Biogenesis, Biological Functions and Their Roles in Diseases. *J Mol Med* 2018,
691 *96*, 1167–1176, doi:10.1007/s00109-018-1693-y.

692 62. Gagnon, K.T.; Corey, D.R. Argonaute and the Nuclear RNAs: New Pathways for RNA-
693 Mediated Control of Gene Expression. *Nucleic Acid Ther* 2012, *22*, 3–16,
694 doi:10.1089/nat.2011.0330.

695 63. Grelet, S.; McShane, A.; Hok, E.; Tomberlin, J.; Howe, P.H.; Geslain, R. SPOt: A Novel and
696 Streamlined Microarray Platform for Observing Cellular TRNA Levels. *Plos One* 2017, *12*,
697 e0177939, doi:10.1371/journal.pone.0177939.

698 64. Kumar, P.; Anaya, J.; Mudunuri, S.B.; Dutta, A. Meta-Analysis of TRNA Derived RNA
699 Fragments Reveals That They Are Evolutionarily Conserved and Associate with AGO Proteins
700 to Recognize Specific RNA Targets. *Bmc Biol* 2014, *12*, 78, doi:10.1186/s12915-014-0078-0.

701 65. Cherlin, T.; Magee, R.; Jing, Y.; Pliatsika, V.; Loher, P.; Rigoutsos, I. Ribosomal RNA
702 Fragmentation into Short RNAs (RRFs) Is Modulated in a Sex- and Population of Origin-
703 Specific Manner. *Bmc Biol* 2020, *18*, 38, doi:10.1186/s12915-020-0763-0.

704 66. Guan, L.; Grigoriev, A. Computational Meta-Analysis of Ribosomal RNA Fragments:
705 Potential Targets and Interaction Mechanisms. *Nucleic Acids Res* 2021, *49*, gkab190-,
706 doi:10.1093/nar/gkab190.

707 67. Sasaki, M.; Nishida, C.; Kodama, Y. Characterization of Silver-Stained Nucleolus Organizer
708 Regions (Ag-NORs) in 16 Inbred Strains of the Norway Rat, Rattus Norvegicus. *Cytogenet*
709 *Genome Res* 1986, *41*, 83–88, doi:10.1159/000132208.

710 68. Goodrich, R.J.; Anton, E.; Krawetz, S.A. Spermatogenesis, Methods and Protocols. *Methods*
711 *Mol Biology* 2012, 385–396, doi:10.1007/978-1-62703-038-0_33.

712 69. Johnson, G.D.; Sendler, E.; Lalancette, C.; Hauser, R.; Diamond, M.P.; Krawetz, S.A.
713 Cleavage of RRNA Ensures Translational Cessation in Sperm at Fertilization. *Mhr Basic Sci*
714 *Reproductive Medicine* 2011, *17*, 721–726, doi:10.1093/molehr/gar054.

715 70. Almiñana, C.; Tsikis, G.; Labas, V.; Uzbekov, R.; Silveira, J.C. da; Bauersachs, S.;
716 Mermillod, P. Deciphering the Oviductal Extracellular Vesicles Content across the Estrous
717 Cycle: Implications for the Gametes-Oviduct Interactions and the Environment of the Potential
718 Embryo. *Bmc Genomics* 2018, *19*, 622, doi:10.1186/s12864-018-4982-5.

719 71. Kowalski, M.P.; Krude, T. Functional Roles of Non-Coding Y RNAs. *Int J Biochem Cell*
720 *Biology* 2015, *66*, 20–29, doi:10.1016/j.biocel.2015.07.003.

721 72. Driedonks, T.A.P.; Hoen, E.N.M.N.-'t Circulating Y-RNAs in Extracellular Vesicles and
722 Ribonucleoprotein Complexes; Implications for the Immune System. *Front Immunol* 2019, *9*,
723 3164, doi:10.3389/fimmu.2018.03164.

724 73. Driedonks, T.A.P.; Mol, S.; Bruin, S. de; Peters, A.-L.; Zhang, X.; Lindenbergh, M.F.S.;
725 Beuger, B.M.; Stalborch, A.-M.D. van; Spaan, T.; Jong, E.C. de; et al. Y-RNA Subtype Ratios in
726 Plasma Extracellular Vesicles Are Cell Type- Specific and Are Candidate Biomarkers for
727 Inflammatory Diseases. *J Extracell Vesicles* 2020, *9*, 1764213,
728 doi:10.1080/20013078.2020.1764213.

729 74. Wolin, S.L.; Steitz, J.A. Genes for Two Small Cytoplasmic Ro RNAs Are Adjacent and
730 Appear to Be Single-Copy in the Human Genome. *Cell* 1983, *32*, 735–744, doi:10.1016/0092-
731 8674(83)90059-4.

732 75. Gardiner-Garden, M.; Frommer, M. CpG Islands in Vertebrate Genomes. *J Mol Biol* 1987,
733 *196*, 261–282, doi:10.1016/0022-2836(87)90689-9.

734 76. Cooper, D.N.; Gerber-Huber, S. DNA Methylation and CpG Suppression. *Cell Differ Dev*
735 1985, *17*, 199–205, doi:10.1016/0045-6039(85)90488-9.

736 77. Bird, A.P. CpG-Rich Islands and the Function of DNA Methylation. *Nature* 1986, *321*, 209–
737 213, doi:10.1038/321209a0.

738 78. Medvedeva, Y.A.; Fridman, M.V.; Oparina, N.J.; Malko, D.B.; Ermakova, E.O.;
739 Kulakovskiy, I.V.; Heinzel, A.; Makeev, V.J. Intergenic, Gene Terminal, and Intragenic CpG
740 Islands in the Human Genome. *Bmc Genomics* 2010, *11*, 48–48, doi:10.1186/1471-2164-11-48.

741 79. Hackenberg, M.; Previti, C.; Luque-Escamilla, P.L.; Carpena, P.; Martínez-Aroza, J.; Oliver,
742 J.L. CpGcluster: A Distance-Based Algorithm for CpG-Island Detection. *Bmc Bioinformatics*
743 2006, *7*, 446–446, doi:10.1186/1471-2105-7-446.

744 80. Aravin, A.; Gaidatzis, D.; Pfeffer, S.; Lagos-Quintana, M.; Landgraf, P.; Iovino, N.; Morris,
745 P.; Brownstein, M.J.; Kuramochi-Miyagawa, S.; Nakano, T.; et al. A Novel Class of Small
746 RNAs Bind to MILI Protein in Mouse Testes. *Nature* 2006, *442*, 203–207,
747 doi:10.1038/nature04916.

748 81. Girard, A.; Sachidanandam, R.; Hannon, G.J.; Carmell, M.A. A Germline-Specific Class of
749 Small RNAs Binds Mammalian Piwi Proteins. *Nature* 2006, *442*, 199–202,
750 doi:10.1038/nature04917.

751 82. Carmell, M.A.; Girard, A.; Kant, H.J.G. van de; Bourc'his, D.; Bestor, T.H.; Rooij, D.G. de;
752 Hannon, G.J. MIWI2 Is Essential for Spermatogenesis and Repression of Transposons in the
753 Mouse Male Germline. *Dev Cell* 2007, *12*, 503–514, doi:10.1016/j.devcel.2007.03.001.

754 83. Aravin, A.A.; Sachidanandam, R.; Bourc'his, D.; Schaefer, C.; Pezic, D.; Toth, K.F.; Bestor,
755 T.; Hannon, G.J. A PiRNA Pathway Primed by Individual Transposons Is Linked to De Novo
756 DNA Methylation in Mice. *Mol Cell* 2008, *31*, 785–799, doi:10.1016/j.molcel.2008.09.003.

757 84. Berninger, P.; Jaskiewicz, L.; Khorshid, M.; Zavolan, M. Conserved Generation of Short
758 Products at PiRNA Loci. *Bmc Genomics* 2011, *12*, 46–46, doi:10.1186/1471-2164-12-46.

759 85. Oey, H.M.; Youngson, N.A.; Whitelaw, E. The Characterisation of PiRNA-Related 19mers
760 in the Mouse. *Bmc Genomics* 2011, *12*, 315–315, doi:10.1186/1471-2164-12-315.

761 86. Ichiyanagi, T.; Ichiyanagi, K.; Ogawa, A.; Kuramochi-Miyagawa, S.; Nakano, T.; Chuma,
762 S.; Sasaki, H.; Udono, H. HSP90α Plays an Important Role in PiRNA Biogenesis and
763 Retrotransposon Repression in Mouse. *Nucleic Acids Res* 2014, *42*, 11903–11911,
764 doi:10.1093/nar/gku881.

765 87. Beyret, E.; Liu, N.; Lin, H. PiRNA Biogenesis during Adult Spermatogenesis in Mice Is
766 Independent of the Ping-Pong Mechanism. *Cell Res* 2012, *22*, 1429–1439,
767 doi:10.1038/cr.2012.120.

768 88. Sullivan, R.; Frenette, G.; Girouard, J. Epididymosomes Are Involved in the Acquisition of
769 New Sperm Proteins during Epididymal Transit. *Asian J Androl* 2007, *9*, 483–491,
770 doi:10.1111/j.1745-7262.2007.00281.x.

771 89. Caballero, J.; Frenette, G.; D'Amours, O.; Belleannée, C.; Lacroix-Pepin, N.; Robert, C.;
772 Sullivan, R. Bovine Sperm Raft Membrane Associated Glioma Pathogenesis-Related 1-like
773 Protein 1 (GliPr1L1) Is Modified during the Epididymal Transit and Is Potentially Involved in
774 Sperm Binding to the Zona Pellucida. *J Cell Physiol* 2012, *227*, 3876–3886,
775 doi:10.1002/jcp.24099.

776 90. Eickhoff, R.; Baldauf, C.; Koyro, H.-W.; Wennemuth, G.; Suga, Y.; Seitz, J.; Henkel, R.;
777 Meinhardt, A. Influence of Macrophage Migration Inhibitory Factor (MIF) on the Zinc Content
778 and Redox State of Protein-Bound Sulphydryl Groups in Rat Sperm: Indications for a New Role
779 of MIF in Sperm Maturation. *Mhr Basic Sci Reproductive Medicine* 2004, *10*, 605–611,
780 doi:10.1093/molehr/gah075.

781 91. Fullston, T.; Teague, E.M.C.O.; Palmer, N.O.; DeBlasio, M.J.; Mitchell, M.; Corbett, M.;
782 Print, C.G.; Owens, J.A.; Lane, M. Paternal Obesity Initiates Metabolic Disturbances in Two
783 Generations of Mice with Incomplete Penetrance to the F2 Generation and Alters the
784 Transcriptional Profile of Testis and Sperm MicroRNA Content. *The FASEB Journal* 2013, *27*,
785 4226–4243.

786 92. Zhang, Y.; Zhang, X.; Shi, J.; Tuorto, F.; Li, X.; Liu, Y.; Liebers, R.; Zhang, L.; Qu, Y.;
787 Qian, J.; et al. Dnmt2 Mediates Intergenerational Transmission of Paternally Acquired Metabolic
788 Disorders through Sperm Small Non-Coding RNAs. *Nat Cell Biol* 2018, *20*, 535–540,
789 doi:10.1038/s41556-018-0087-2.

790 93. Rodgers, A.B.; Morgan, C.P.; Leu, N.A.; Bale, T.L. Transgenerational Epigenetic
791 Programming via Sperm MicroRNA Recapitulates Effects of Paternal Stress. *Proc National*
792 *Acad Sci* 2015, *112*, 13699–13704, doi:10.1073/pnas.1508347112.

793 94. Short, A.K.; Yeshurun, S.; Powell, R.; Perreau, V.M.; Fox, A.; Kim, J.H.; Pang, T.Y.;
794 Hannan, A.J. Exercise Alters Mouse Sperm Small Noncoding RNAs and Induces a
795 Transgenerational Modification of Male Offspring Conditioned Fear and Anxiety. *Transl*
796 *Psychiat* 2017, *7*, e1114–e1114, doi:10.1038/tp.2017.82.

797 95. Wang, Y.; Chen, Z.-P.; Hu, H.; Lei, J.; Zhou, Z.; Yao, B.; Chen, L.; Liang, G.; Zhan, S.; Zhu,
798 X.; et al. Sperm MicroRNAs Confer Depression Susceptibility to Offspring. *Sci Adv* 2021, *7*,
799 eabd7605, doi:10.1126/sciadv.abd7605.

800 96. Belleannée, C.; Calvo, E.; Thimon, V.; Cyr, D.G.; Légaré, C.; Garneau, L.; Sullivan, R. Role
801 of MicroRNAs in Controlling Gene Expression in Different Segments of the Human Epididymis.
802 *Plos One* 2012, *7*, e34996, doi:10.1371/journal.pone.0034996.

803 97. Kierszenbaum, A.L.; Tres, L.L. Structural and Transcriptional Features of the Mouse
804 Spermatid Genome. *J Cell Biology* 1975, *65*, 258–270, doi:10.1083/jcb.65.2.258.

805 98. Hecht, N.B. Molecular Mechanisms of Male Germ Cell Differentiation. *Bioessays* 1998, *20*,
806 555–561, doi:10.1002/(sici)1521-1878(199807)20:7<555::aid-bies6>3.0.co;2-j.

807 99. Steger, K. Transcriptional and Translational Regulation of Gene Expression in Haploid
808 Spermatids. *Anat Embryol* 1999, *199*, 471–487, doi:10.1007/s004290050245.

809 100. Fischer, B.E.; Wasbrough, E.; Meadows, L.A.; Randlet, O.; Dorus, S.; Karr, T.L.; Russell,
810 S. Conserved Properties of Drosophila and Human Spermatozoal MRNA Repertoires. *Proc*
811 *Royal Soc B Biological Sci* 2012, *279*, 2636–2644, doi:10.1098/rspb.2012.0153.

101. Chen, T.; Chen, X.; Zhang, S.; Zhu, J.; Tang, B.; Wang, A.; Dong, L.; Zhang, Z.; Yu, C.; Sun, Y.; et al. The Genome Sequence Archive Family: Toward Explosive Data Growth and Diverse Data Types. *Genom Proteom Bioinform* 2021, *19*, 578–583, doi:10.1016/j.gpb.2021.08.001.

102. Xue, Y.; Bao, Y.; Zhang, Z.; Zhao, W.; Xiao, J.; He, S.; Zhang, G.; Li, Y.; Zhao, G.; Chen, R.; et al. Database Resources of the National Genomics Data Center, China National Center for Bioinformation in 2022. *Nucleic Acids Res* 2021, *50*, D27–D38, doi:10.1093/nar/gkab951.

103. Weng, Q.; Wang, Y.; Xie, Y.; Yu, X.; Zhang, S.; Ge, J.; Li, Z.; Ye, G.; Guo, J. Extracellular Vesicles-Associated TRNA-Derived Fragments (TRFs): Biogenesis, Biological Functions, and Their Role as Potential Biomarkers in Human Diseases. *J Mol Med* 2022, 1–17, doi:10.1007/s00109-022-02189-0.

104. R Core Team. *R: A Language and Environment for Statistical Computing*; R Foundation for Statistical Computing: Vienna, Austria, v4.2.0; 2022.

105. Phanstiel, D.H. *Sushi: Tools for Visualizing Genomics Data*; v1.34.0; 2022.

106. Corral-Vazquez, C.; Salas-Huetos, A.; Blanco, J.; Vidal, F.; Sarrate, Z.; Anton, E. Sperm MicroRNA Pairs: New Perspectives in the Search for Male Fertility Biomarkers. *Fertil Steril* 2019, *112*, 831–841, doi:10.1016/j.fertnstert.2019.07.006.

107. Sun, J.; Zhao, Y.; He, J.; Zhou, Q.; El-Ashram, S.; Yuan, S.; Chi, S.; Qin, J.; Huang, Z.; Ye, M.; et al. Small RNA Expression Patterns in Seminal Plasma Exosomes Isolated from Semen Containing Spermatozoa with Cytoplasmic Droplets versus Regular Exosomes in Boar Semen. *Theriogenology* 2021, *176*, 233–243, doi:10.1016/j.theriogenology.2021.09.031.

108. Alves, M.B.R.; Celeghini, E.C.C.; Belleannée, C. From Sperm Motility to Sperm-Borne MicroRNA Signatures: New Approaches to Predict Male Fertility Potential. *Frontiers Cell Dev Biology* 2020, *8*, 791, doi:10.3389/fcell.2020.00791.

109. Liu, W.-M.; Pang, R.T.K.; Chiu, P.C.N.; Wong, B.P.C.; Lao, K.; Lee, K.-F.; Yeung, W.S.B. Sperm-Borne MicroRNA-34c Is Required for the First Cleavage Division in Mouse. *Proc National Acad Sci* 2012, *109*, 490–494, doi:10.1073/pnas.1110368109.

841 **FIGURES**

842 **Figure 1.**

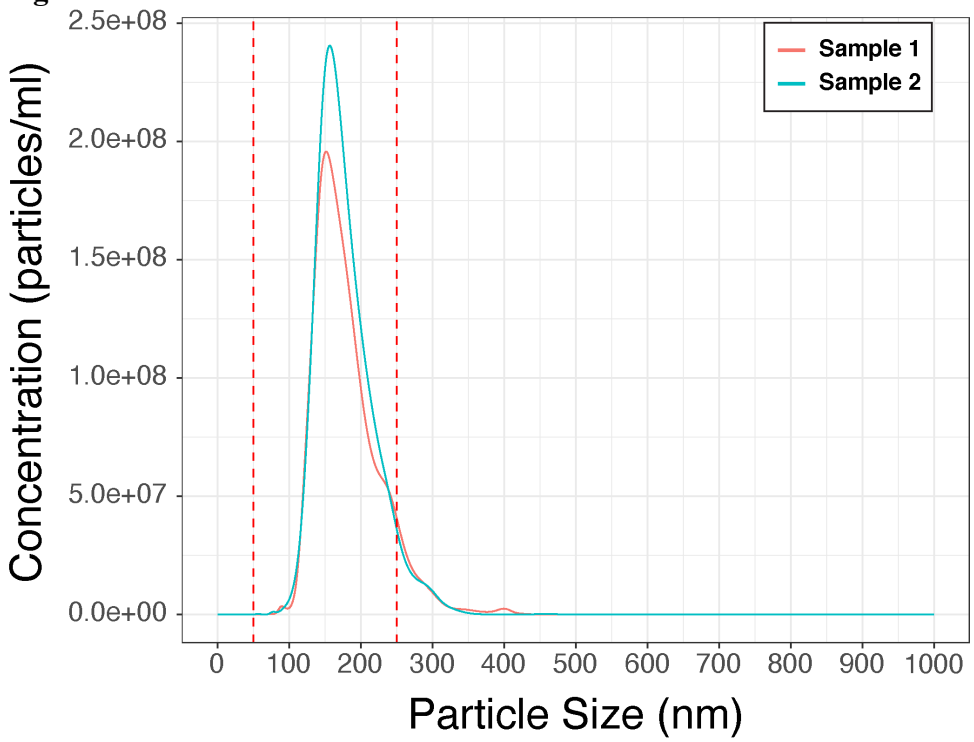

843

844 The size distribution and density of the extracellular vesicles from two separate samples are
845 shown as analyzed by nano-particle tracking (NanoSight 300). The red dashed lines indicate the
846 boundaries of size for canonical epididymosomes (50 – 250 nm [4]).

847

848 **Figure 2.**

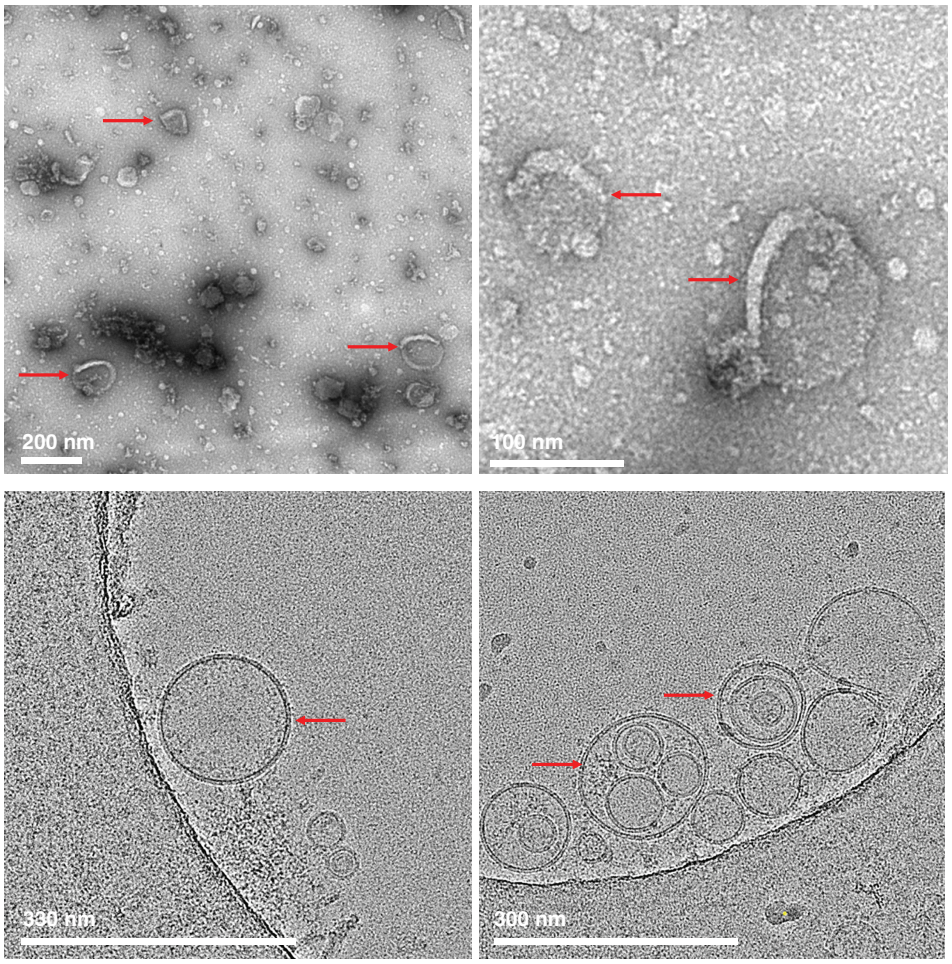

849
850
851 Results from imaging EPs from the rat caput are shown. **A, B)** Representative TEM images of
852 our EP preparation. Red arrows point to several cup-shaped vesicles, typical of EV morphology.
853 **C)** Cryo-EM image of our EP preparation with an arrow pointing towards a single vesicle. **D)**
854 Arrows point towards multilayer vesicles.

855 **Figure 3.**
856

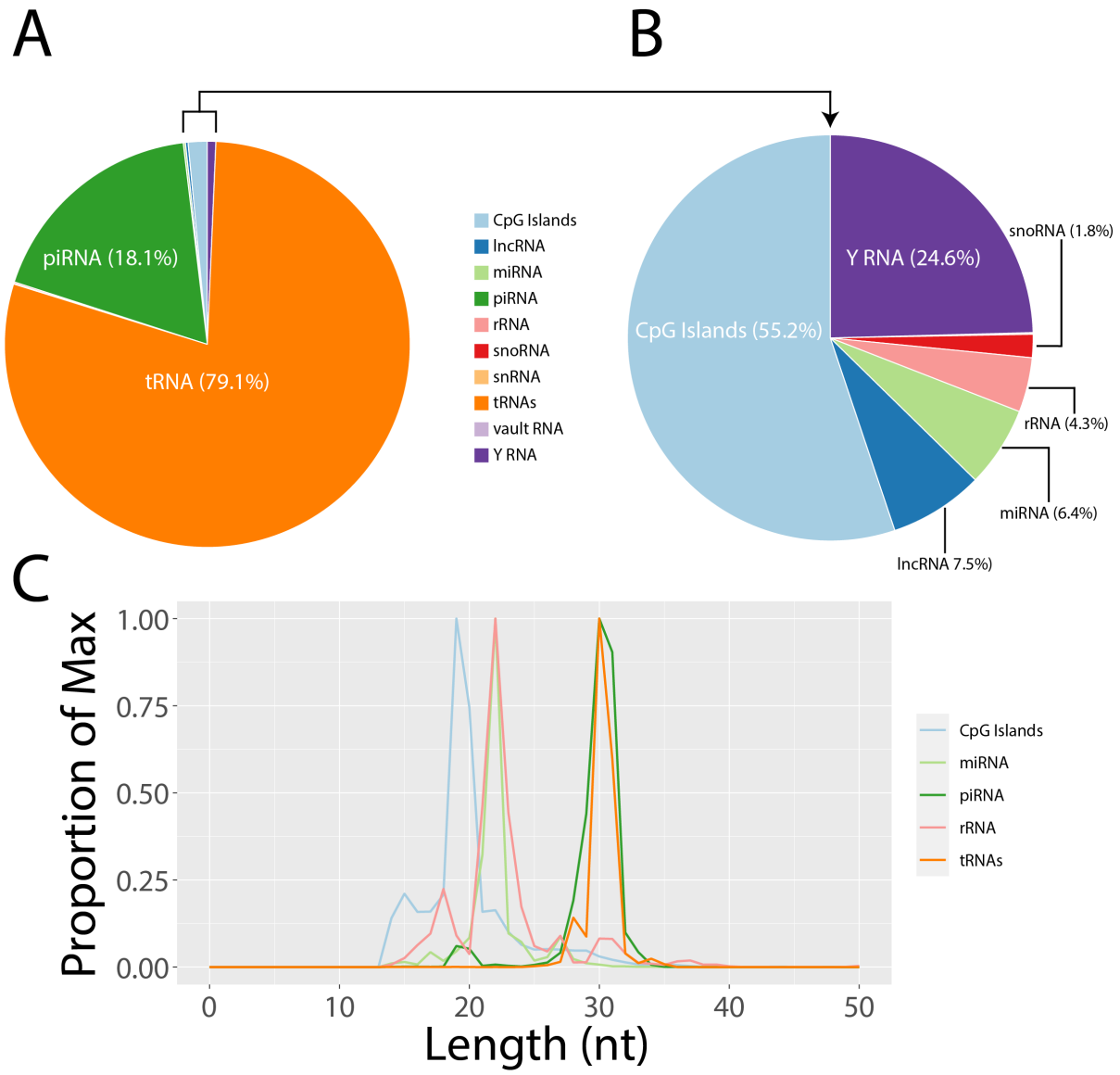

857
858 Results from sequencing small RNAs derived from EVs in the rat caput are shown. **A)** The
859 proportion of small RNA reads assigned to each of 10 annotations in our analysis; tRNA and
860 piRNA account for the 97.2% of small RNA in caput EVs while miRNAs only account for
861 0.177%. **B)** The remaining small RNA reads are shown as a proportion of the residual 2.8% not
862 assigned to tRNA or piRNA loci. CpG islands, which are not a known unit of small RNA
863 expression, account for the majority (55.2%) of the remaining reads. **C)** The size distribution of 4
864 well-defined sncRNAs are shown together with the one undefined category (CpG islands); the
865 latter has a unique size profile (19 nt). The size distribution for piRNA (29-31 nt) and miRNA
866 (22 nt) are exactly as expected [51,52]. Reads aligned to tRNA (30 - 31 nt) and rRNA (primary
867 peak at 22 nt and small peaks at 18 nt and 30 nt) both demonstrate expected size specific
868 fragmentation [65,103].

869 **Figure 4.**

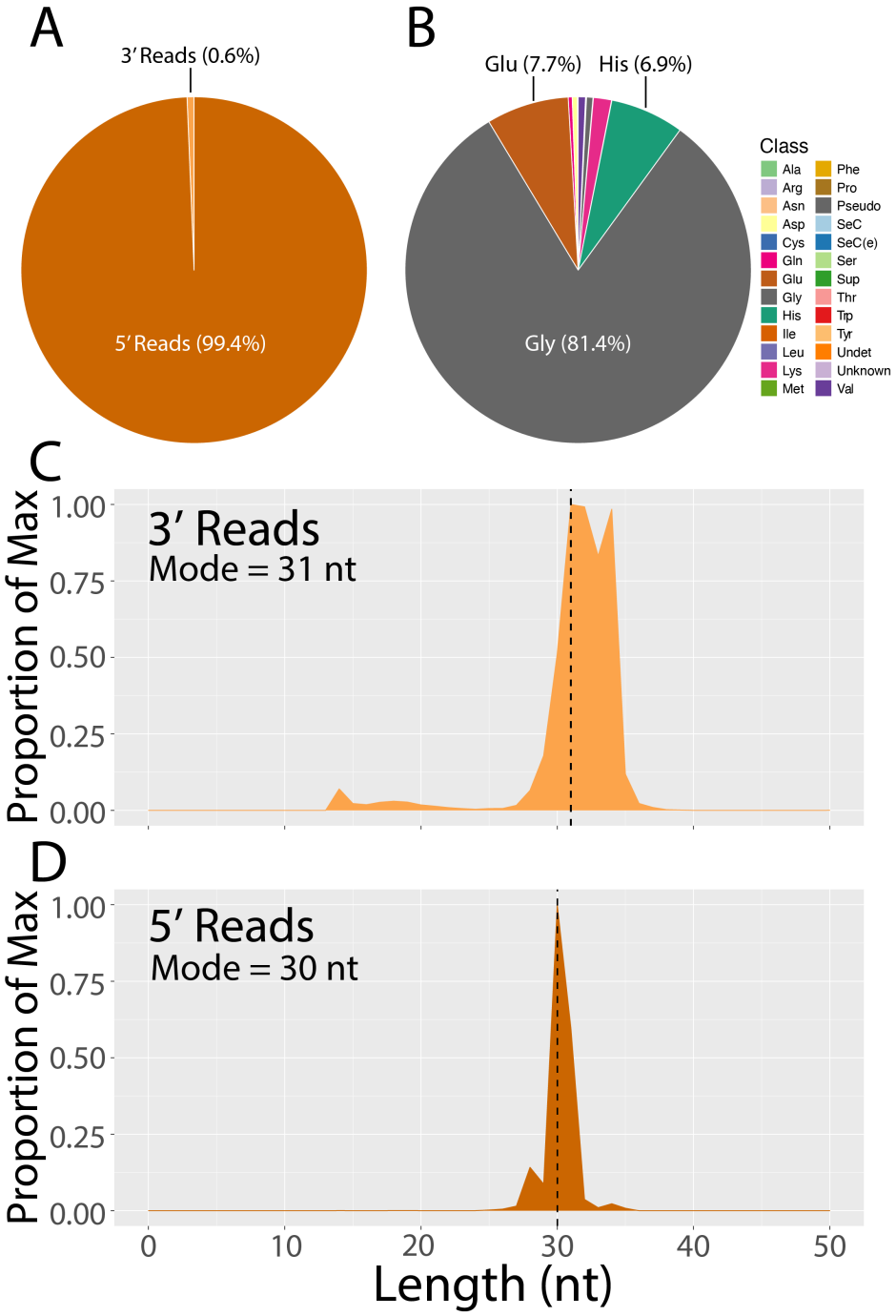

870
871 Detailed analysis of tRNA reads is shown. **A)** Reads align to the 5' end of tRNA loci almost
872 exclusively. **B)** 5'-tRNA^{Gly} is the primary tRNA fragment found in rat caput extracellular
873 vesicles, followed by a substantially smaller proportion of 5'-tRNA^{Glu} and 5'-tRNA^{His}. **C-D)** The
874 size distribution of 3' and 5' tRNA reads are shown, respectively. Reads from the 3' end of
875 tRNA are slightly longer and have a broader distribution.

876 **Figure 5.**

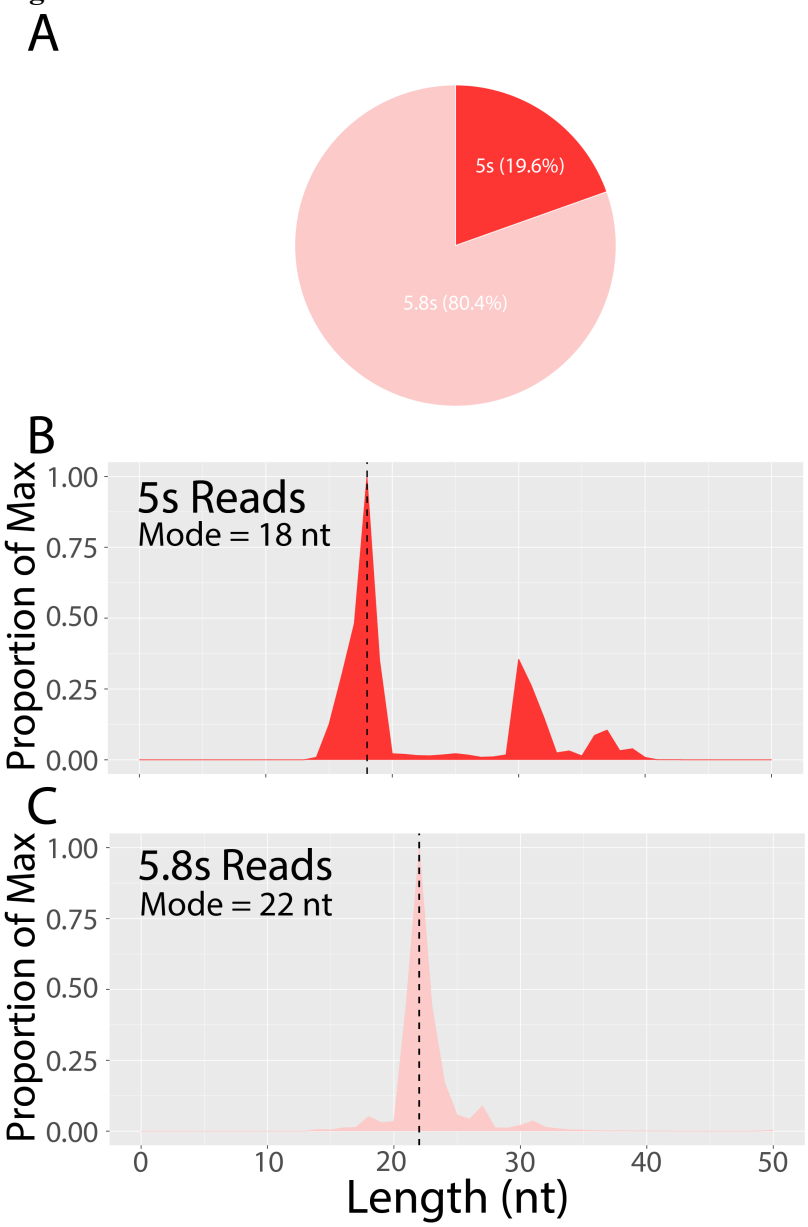

877
878 Reads that aligned to annotated rRNA loci are shown by subcategory. The rat genome is poorly
879 annotated for rRNA, so the available 5s and 5.8s loci were used for categorization. **A)** The
880 majority of rRNA reads aligned to 5.8s rRNA. **B-C)** The size distribution for reads aligned to 5s
881 and 5.8s rRNA show profiles indicative of rRFs that are distinct from one another. **B)** 5s rRFs
882 show a bimodal distribution with peaks at 18 and 30 nt. **C)** 5.8s rRFs show a single peak at 22 nt.

883 **Figure 6**

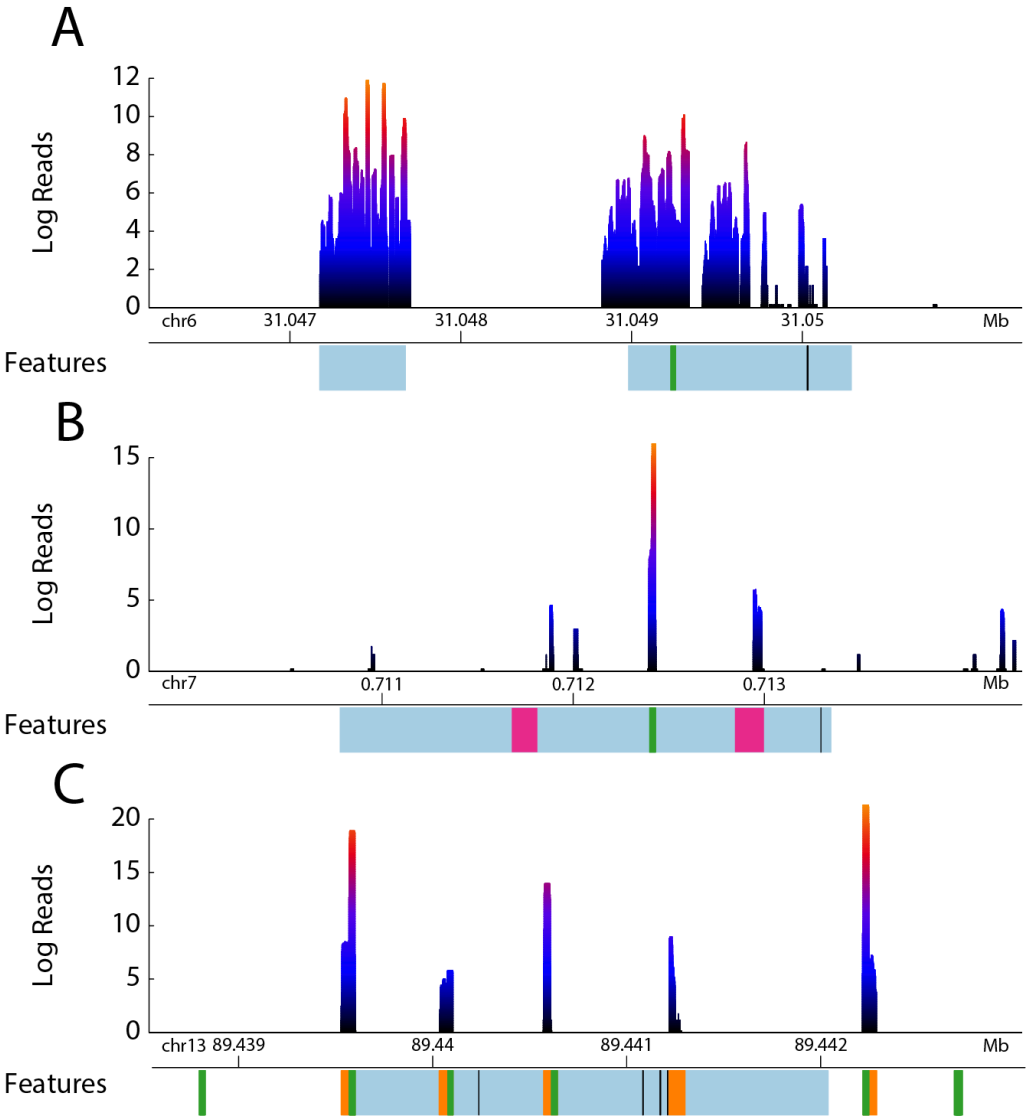

884
885 The log transformed density of reads is shown across three CpG islands with different
886 characteristics. Feature annotations are shown below the x-axis and are indicated by color as
887 follows: Light blue designates a CpG island; Green = piRNA, Black = predicted transcriptional
888 start sites, Pink = 5.8s rRNA, and orange = tRNA. The density of reads is indicated by a heat
889 map from black (minimum) to red (maximum) scaled to each respective y-axis. Plots were
890 generated from BedGraph files with R (v4.2.0 [104]) and the Sushi package (v1.34.0,
891 http://bioconductor.riken.jp/packages/3.1/bioc/html/Sushi.html [105]). **A)** Reads are shown
892 expressed from within the boundaries of a CpG island on chromosome 6. The reads within the 3'
893 CpG island were not associated with the piRNA (green), while the 5' CpG island had no other
894 overlying features. **B)** Reads were identified within a CpG island on chromosome 7 but the
895 majority of them aligned to a piRNA (green) and rRNA (pink) feature. **C)** Reads were identified
896 within a CpG island on chromosome 13 but they aligned exclusively to piRNA and tRNA loci
897 and are demonstrative of their typical expression profiles. The CpG islands from **B & C** (and all
898 other CpG islands such as these) were removed from the analysis of small RNAs expressed from
899 CpG islands. The two in **A** are representative of those that were used for further analysis.

Figure 7

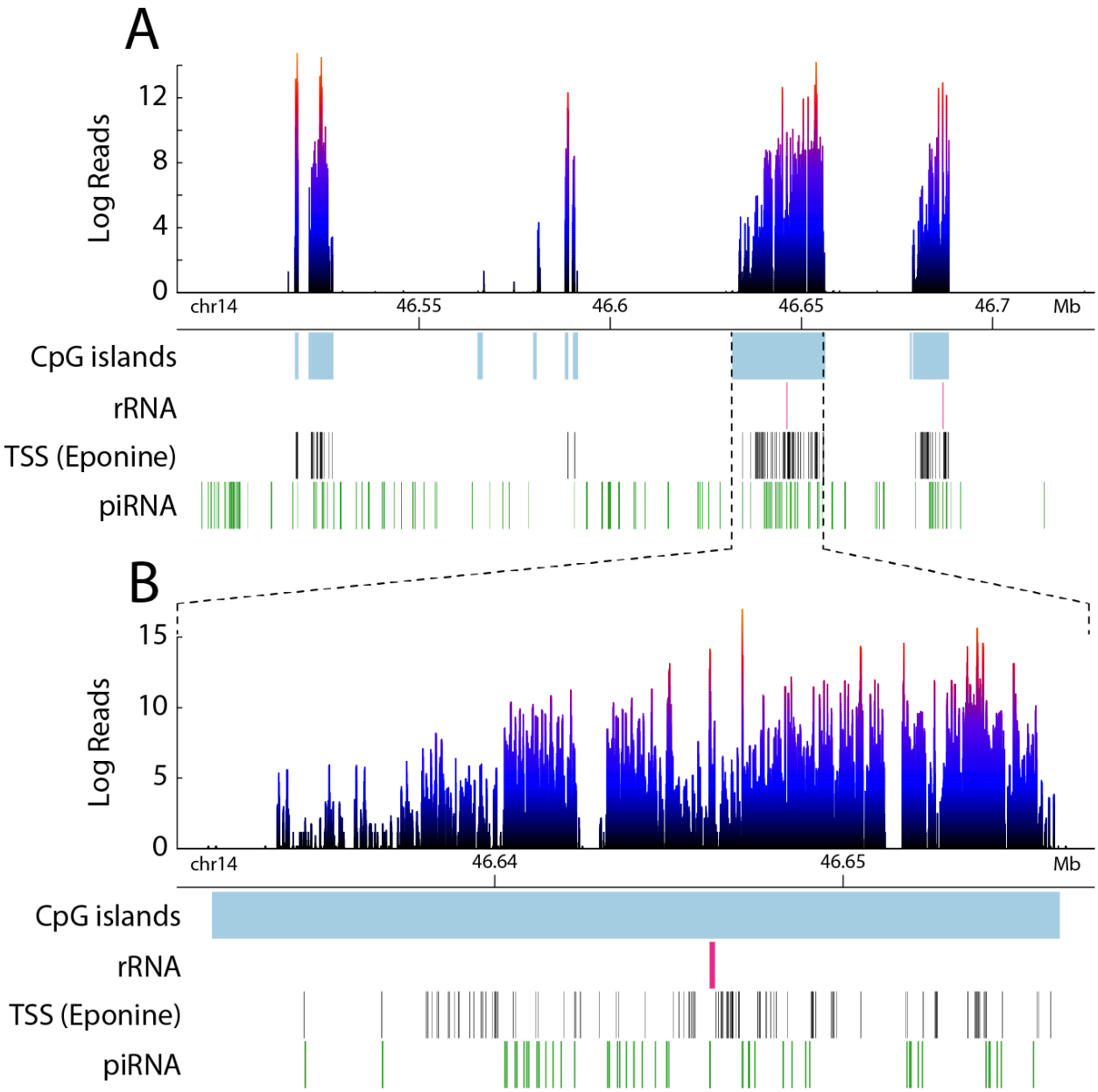

The log transformed reads from a cluster of 8 CpG islands on chromosome 14 are shown with the primary overlying features indicated by color and label below the x-axis. Light blue designates the CpG islands. Pink = 5.8s rRNA, Black = predicted transcriptional start sites, Green = piRNA. The density of reads is indicated by a heat map from black (minimum) to red (maximum) scaled to each respective y-axis. Plots were generated from BedGraph files with R (v4.2.0 [104]) and the Sushi package (v1.34.0, http://bioconductor.riken.jp/packages/3.1/bioc/html/Sushi.html [105]). **A)** The boundaries of the reads shown are clearly demarcated by CpG islands and could not be attributable to overlying features such as rRNA or piRNA. **B)** A detailed view of the largest CpG island in the chromosome 14 cluster. The reads are not associated with either the rRNA or piRNA features within the CpG island and are unique from those found elsewhere (Figure 5B & C).

913 **TABLES**

914 **Table 1**

915

Class	% of Total	Mode	Median	Mean	SD	90% Range (nt)
tRNAs	79.124	30	30	30.19	1.18	28 - 31
piRNA	18.125	30	30	29.6	2.5	26 - 32
CpG Islands	1.518	19	19	19.89	3.75	15 - 28
Y RNA	0.676	31	31	28.33	3.89	22 - 31
lncRNA	0.207	22	22	22.27	4.98	15 - 33
miRNA	0.177	22	22	22.04	2.34	19 - 27
rRNA	0.12	22	22	22.65	4.06	17 - 31
Vault RNA	0.001	18	19	22.99	8.02	14 - 41
snRNA	0.003	16	16	18.05	3.85	15 - 26
snoRNA	0.051	27	24	23.44	5.12	15 - 32

916

917 Descriptive statistics of the proportion and read length for each annotated small RNA category
918 are shown, with the mode, median, mean, standard deviation, and length range from which 90
919 percent of the reads are found. Data are a composite of the 6 individuals.

920 **Table 2**

921

Class	All (%)	OPA16A (%)	OPA21C (%)	OPA24A (%)	OPA31A (%)	OPA22A (%)	OPA23B (%)
tRNAs	79.124	76.084	78.923	80.168	81.334	79.366	78.128
piRNA	18.125	20.219	18.729	17.272	16.739	17.463	18.705
CpG islands	1.518	2.567	1.273	1.155	1.042	1.518	1.796
Y RNA	0.676	0.404	0.627	0.903	0.487	0.993	0.673
lncRNA	0.207	0.255	0.169	0.184	0.153	0.241	0.300
miRNA	0.177	0.251	0.146	0.172	0.135	0.224	0.207
rRNA	0.120	0.177	0.087	0.092	0.075	0.130	0.097
Vault RNA	0.001	0.000	0.001	0.001	0.001	0.001	0.002
snRNA	0.003	0.003	0.002	0.002	0.002	0.004	0.004
snoRNA	0.051	0.040	0.044	0.051	0.032	0.060	0.088

922

923

924 Distribution of the percentages represented by the small RNA categories in the six individual rat
925 caput epididymis EP samples (individual rat identifiers, with the prefix OPA, are provided).
926 There was considerable consistency across the six individuals.

927 **Table 3**

Name	Reads per Million	Found in Sperm	Found in EVs
miR-1b	16.2	--	--
miR-7a-1	19.7	[106]	[107]
miR-7a-2	19.9	[106]	[107]
miR-let-7c	10.0	[106]	[107]
miR-let-7i	11.7	[106]	[107]
miR-26a	11.7	[108]	--
miR-99a	87.8	[109]	--
miR-143	29.5	[22]	[22]
miR-148a	93.0	[106]	[107]
miR-184	493.7	[106]	[107]
AABR07005004.2	16.0		
AABR07029907.2	34.7		
AABR07057421.1	11.9		
AABR07064716.2	34.2		
AABR07064724.1	22.1		

928

929 Fifteen miRNA were identified as having substantial (> 10 RPM) expression in rat caput EVs, 10
930 of which are annotated and 5 that are putative. This is far fewer than expected based on mouse
931 experiments [34]. The majority of miRNAs identified have previously been reported in either
932 sperm or EVs, except for miR-1b. A miRNA considered a hallmark of caput EVs (miR-143) was
933 also identified in our rat data set.

934 **Table 4**.

Chromosome	Start Location	End Location	Length (nt)	Read Count	RPKM	piRNA Loci	pRNA Protein Loci	rRNA Binding Protein Loci	rRNA Loci
Chr 1	11,903,555	11,916,838	13,283	112,070	63.16	19	1	0	1
Chr 1	11,961,297	11,975,108	13,811	278,633	151.02	27	1	0	1
Chr 5	91,124,274	91,141,016	16,742	341,585	152.72	26	1	0	1
Chr 6	30,627,068	30,633,859	6,791	177,949	196.15	13	0	0	2
Chr 6	31,047,175	31,047,676	501	10,347	154.59	0	0	0	0
Chr 6	31,048,983	31,050,286	1,303	3,282	18.85	1	0	0	0
Chr 14	46,517,594	46,518,401	807	113,831	1,055.86	1	0	0	0
Chr 14	46,521,126	46,527,599	6,473	170,612	197.30	10	0	1	0
Chr 14	46,588,206	46,589,034	828	39,955	361.21	0	0	1	0
Chr 14	46,590,294	46,591,521	1,227	2,562	15.63	1	0	1	0
Chr 14	46,631,880	46,656,213	24,333	429,235	132.04	44	0	1	1
Chr 14	46,679,234	46,688,547	9,313	160,403	128.93	17	0	0	1

935

936 The genomic coordinates (Rnor v6 – Chromosome, Start Location, End Location) of 12 CpG
937 islands found to have substantial expression (> 10 RPKM) of ~19 nt small RNA transcripts are
938 shown along with the length of the CpG island, raw read count, and length-corrected read count
939 (RPKM) found within each. The number of features found overlapping each CpG island is also
940 shown.